First-Principles Electronic-Structure Calculations of Functional Materials

First-Principles Electronic-Structure Calculations of Functional Materials

Jianbo Lin

July 2014

Dissertation

First-Principles Electronic-Structure Calculations of Functional Materials

Graduate School of Natural Science & Technology
Kanazawa University

Major subject: Division of Mathematical and Physical Sciences

Course: Computational Science

School registration No. 1123102014

Name: Jianbo Lin

Chief advisor: Mineo Saito

Abstract

The control of materials on the atomic level is necessary for development of devices which are essential in information technology. Then simulation based on quantum mechanics becomes important. In the study, we take two topics.

One is control of defects in graphene. Recently, a low-energy electron irradiation experiment introduced some unknown defects on single-walled carbon nanotubes(SWCNTs)[28]. Meanwhile, hydrogen thermal desorption spectroscopy treat these defects which are healed at 44-70K[31]. This defect is assumed to be adatom-vacancy pair. As experimental methods are not sufficient to investigate the atomic phenomenon, we do the computational study by first-principles calculations of adatom-vacancy pair defects on graphene which is a SWCNT with infinite radius. We found that the healing barrier of the adatom-vacancy pair is very small (0.06 eV) when the adatom is bonded to a nearest carbon atom of the mono-vacancy. Therefore, this pair is easily healed. On the other hand, the healing barrier becomes high (0.24-0.32 eV) when the adatom is located 4.26-5.54 Å far from the vacant site, but these barriers are lower than that of the adatom diffusion. Therefore, it is expected that these adatom-vacancy pairs are healed in low temperature range where the adatom does not diffuse.

The other is spin-polarization in ferromagnetic materials. As the developing of technology of spintronics, it is essential to find some effective tools to measure the spin-polarization of the magnetic material. However, the measurement methods are still rare. A recent experimental study by using Doppler broadening of annihilation radiation [34, 35] showed that there are observable difference of the distributions of majority electrons and minority electrons in ferromagnetic metals. It is still unknown what kind of useful information we can get from this

experiment results. We try the first-principles calculation to find the if there is useful information that can contribute to spintronics. We also confirm the reliability of the electron-positron DFT which is used to perform the positron annihilation calculations. The calculations are carried out on the ferromagnetic metals (Fe, Co, and Ni). We found that the lifetime differences ($\tau^{\downarrow} - \tau^{\uparrow}$) are 11.85 ps, 3.75 ps, -4.36 ps, and for Fe, Co, and Ni, respectively. The positive values for Fe and Gd, and the negative value for Ni are consistent with results of 3γ experiment[37]. The origin of the negative sign is expected from the delocalized distribution of minority electron which contributes much to the overlap of electron-positron. Thus, it is expected that when the magnetic material has small magnetic momentum, the negative lifetime difference is possible to appear. The spin-polarized positron annihilation spectroscopy is expected to have good application in the field of spintronics.

List of Publications

1. **Jianbo Lin**, Kazunori Nishida, and Mineo Saito: *First-Principles Calculation of Adatom-Vacancy Pairs on the Graphene.*: Japanese Journal of Applied Physics Vol. 51, pp: 125101, September 2012..

2. **Jianbo Lin**, Takahiro Yamasaki, and Mineo Saito: *Spin polarized positron lifetimes in ferromagnetic metals: First-principles study.*: Japanese Journal of Applied Physics Vol. 53, pp 053002, April 2014.

Dedication

Dedicated to my Mother and Father.

Contents

Abstract i

List of Publications iii

Dedication iv

List of Figures viii

List of Tables x

1 Introduction 1

1.1 Importance of Device Study 1

1.2 Why First-Principles Calculation is Necessary 2

1.3 Scope of This Study 3

1.3.1 Adatom-Vacancy Pair Defect in Graphene 3

1.3.2 Positron Annihilation Study on Ferromagnetic Metals 4

1.4 Structure of The Thesis 6

2 Theory and Calculational Details 7

2.1 Theoretical Background 8

2.1.1 Variation Principle 9

2.1.2 Hartree-Fock Approximation 11

2.2 Density Functional Theory (DFT) 14

2.2.1 Hohenberg-Kohn Theorems 14

2.2.2 Kohn-Sham equations 16
2.3 Exchange and Correlation Functional 19
2.3.1 Local Density Approximation (LDA) 19
2.3.2 Generalized Gradient Approximation (GGA) 21
2.4 Plane Waves Method 22
2.5 Pseudopotential 23
2.5.1 Norm Conserving Pseudopotential 24
2.5.2 Ultrasoft Pseudopotential 24
2.6 Formation Energy and Energy Barrier 26
2.7 Electron-Positron Density Functional Theory (EPDFT) 27
2.8 Calculation Details 28

3 Healing of Adatom-vacancy Pair Defects in Graphene 30
3.1 Introduction 30
3.2 The Adatom Bonded to A Nearest Atom of The Vacancy Site 32
3.3 The Adatom Bonded to An Atom Which is 4.26-5.54 Å Far From The Vacancy Site 34
3.4 Analysis of Spin Density of Adatom-Vacancy Pair Defects 35
3.5 Discussion 36

4 Positron annihilation studies on ferromagnetic metals 39
4.1 Introduction 39
4.2 Non-spin-polarized case 40
4.3 Spin-polarized case 41
4.4 Explanations for the negative lifetime difference ($\tau^{\downarrow}$-$\tau^{\uparrow}$) in Ni 42
4.5 Conclusion 47

5 Summary 50
5.1 Conclusions 50
5.1.1 Adatom-Vacancy Pair Defects in Graphene 50

5.1.2 Positron Annihilation Study on Ferromagnetic Metals 51
5.2 Future Scope 52
5.2.1 Study of Atomic Defect in Functional Materials 52
5.2.2 Study of Spin-Polarized Positron Annihilation for Spintronics 53

References **54**

Acknowledgments **59**

List of Figures

1.1 Silicon crystal and semiconductor transistor. 1

1.2 Spin of elecron and its application. 5

1.3 Positron annihilation in bulk metal. 5

2.1 The constrained optimization method for energy barrier 26

2.2 The energy barrier 27

3.1 Adatom-vacancy pair when the adatom is bonded to a nearest site of the vacancy in the graphene. 32

3.2 Formation energies of the adatom-vacancy pairs in the graphene. 33

3.3 Healing path of geometry C and D. Geometry C and geometry D are shown in (a) and (c), respectively. Two transition states are shown in (b) and (d). 35

3.4 Adatom-vacancy pair when the atom little (5.54 Å) far from the vacancy in graphene (a) and the transition geometry (b). 36

3.5 Magnetic property of adatom-vacancy pair. 37

4.1 Atomic projected density of states. 43

4.2 Spin density of states:(a)Fe, (b)Co, and (c)Ni. 44

4.3 Spin densities of electron ((a) and (b) with the different color bars as left and right), density of the positron (d), and electron-positron overlaps ((f) and (g)) in the case of Ni of the [110] direction. The units in (a), (b), and (d) are $e/(au)^3$, and those in (f) and (g) are $e^2/(au)^6$, respectively. 45

4.4 Spin densities of electron ((a) and (b) with different color bar as up and down), density of the positron (d), and electron-positron overlaps ((f) and (g)) in the case of Fe of the [110] direction. The units in (a), (b), and (d) are $e/(au)^3$, and those in (f) and (g) are $e^2/(au)^6$, respectively. 46

4.5 Spin densities of electron ((a) and (b)), density of the positron (d), and electron-positron overlaps ((f) and (g)) in the case of Co of the [0100] direction. The units in (a), (b), and (d) are $e/(au)^3$, and those in (f) and (g) are $e^2/(au)^6$, respectively. 47

4.6 Spin densities of electron ((a) and (b)), density of the positron (d), and electron-positron overlaps ((f) and (g)) in the case of Gd of the [0100] direction. The units in (a), (b), and (d) are $e/(au)^3$, and those in (f) and (g) are $e^2/(au)^6$, respectively. 48

5.1 Defects in graphene. 52

List of Tables

4.1 Non-spin-polarized positron lifetimes (ps) for the bulk Fe, Ni, and Co. 40

4.2 Spin-polarized positron lifetimes for the bulk Fe (bcc), Co (hcp), Ni (fcc), and Gd (hcp). We also show the spin moments ($\mu B/atom$). 41

4.3 $P^{3\gamma}$ from three photon polarization measurement 42

Chapter 1

Introduction

1.1 Importance of Device Study

Nowadays, electronic products, such as computers, mobile phones, televisions, and so on, are necessary in our daily life. In these products, the semiconductor devices are commonly used (shown in Fig.1.1). So, the study of device is important. As a result of efforts by researchers and engineers, the developing of the semiconductor technology is so fast almost as same as the Moore's Law predicted.

Then, the widely used Si-based semiconductor device is developing because of the down-

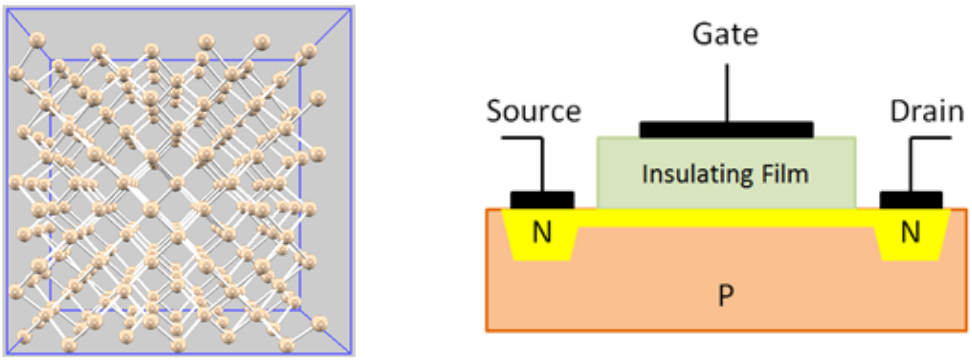

(a) Silicon crystal

(b) Semiconductor transistor

Figure 1.1: Silicon crystal and semiconductor transistor.

sizing to several nano-meters. However, this Si-based semiconductor device is considered to reach its performance limitation soon. Thus, it is necessary to find and study new functional materials for the future device.

1.2 Why First-Principles Calculation is Necessary

Electronic devices are widely used in the information technology field because of the application of the electrons. The properties of electrons determine the properties of functional materials. Then, it is important to study the electron properties of these materials. Therefore simulation of electronic properties is important. This simulation is based on quantum mechanics as mentioned below.

Electrons are the fundamental particles which are contained in the matter around our daily life (atoms, molecules, condensed matter, and man-made structures). Electrons are very important: not only electrons form the ”quantum glue” that holds together the nuclei in solid, liquid, and molecular states, but also electron excitations determine the electrical, optical, and magnetic properties of materials.[1]

Since the electron was discovered in 1896-1897, the theory of electrons in matter has been a great challenge of theoretical physics. In the beginning, the electrons were considered to be particles, and later they were considered to be waves, then finally the electrons show the wave-particle duality which is also applicable for other matter. Meanwhile, the developing of understanding and the computational methods for electrons allows us to accurately treat the electron-nuclei system in condensed matter and molecules. The density functional theory (DFT), the quantum molecular dynamics, the tight-binding theory, the treatment of psedopotentials, and so on, are applied to solve the properties of electrons in materials. In this thesis, these methods applied to our studies will be mentioned in chapter 2.

As the downsizing of electronic device, atomic understanding of electron properties becomes necessary. The methods above allow us to get information on electrons in materials which leads us to understand the atomic phenomenons of the objects. It contributes to devel-

opment of material science if there is some progress on the understanding of the materials for device.

1.3 Scope of This Study

According to the Moore's Law, in the future, the size of semiconductor device will be smaller and smaller. In about 20 years, the carbon nano-materials (fullerene, carbon nanotubes, graphene, and so on), with there low dimensional electronic properties, are expected to be suitable candidates for electronic device. On the other hand, in about 30 years, spin will probably be applied to nano-device which need the technology of spintronics. So, it is necessary to study the topics related to carbon materials and spintronics.

In this study, we choose two topics. One is the defect in graphene which is related to carbon materials; the other is the spin-polarization in ferromagnetic materials which is related to magnetic materials. The backgrounds of these two topics will be mentioned as below.

1.3.1 Adatom-Vacancy Pair Defect in Graphene

As above mentioned, possible functional materials for new device are carbon nano-materials, such as fullerene, carbon nanotubes, graphene, and so on. Compared with conventional silicon devices, the effects of defects on carbon nano-device are expected to be serious because of the low dimensional conductivity. Thus, control of defects and impurities on the atomic level is important.

Thus far, pentagon-hexagon pairs [15], mono- and multi-vacancies [16, 17, 18, 19, 20, 21, 22], adatoms [23, 24], adatom dimers [25], and adatom-vacancy pairs [26] have been studied.

Among various defects, adatom related defects were observed at low temperatures. Recently low-energy electron irradiation on single-walled carbon nanotubes (SWCNTs) was performed[28]. The observation of I-V characteristic shows that some defects having some band gaps are created at low temperature by irradiation. Scanning tunneling microscope (STM) with the bias of 4.5 V at low temperature (95 K) also induces some unknown defects having band gaps[29, 30].

These defects are expected to be related to adatoms which can be created by electron irradiation or STM. Then, a hydrogen thermal desorption spectroscopy treat the defects induced by low-energy electron irradiation in SWCNTs. And it shows that some defects are healed at 44-70 K[31]. It is expected that the observed defect was the adatom-vacancy pair. It is emerge to have a theoretical study to understand this kind of defect better. The experimental methods are considered to be not so sufficient to observe the atomic phenomenon. However, the computational methods are expected to study these problems much efficiently.

The experimental studies show that there are temperature dependence for creating defects in CNTs. However, the experimental studies did not give information on formation energy and healing barrier of the defects. So, the purpose of this study is to investigate the energetic stable structures and the healing barriers of adatom-vacancy pairs. Then, we would like to discuss the stability of the adatom-vacancy pair defects and also to make sure if the adatom tends to return to the vacant site or to immigrate to other position.

The detail of this topic will show in the following chapters.

1.3.2 Positron Annihilation Study on Ferromagnetic Metals

As the previously mentioned, spintronics developed rapidly in recent years which are also considered to be suitable for nano device application in the future. Nowadays, the charge of electron is widely utilized for electronic devices. Spintronics is a technology which is considered to control the spin of electron(Fig.1.2.a). As an example, in Fig.1.2.b, we show that if one can control the spin direction in the ferromagnetic materials, the bit information (1 or 0) can be stored.

Many materials such as ferromagnetic material, half-metal, and so on, are considered to have applications with spintronics on nano devices. As an important parameter, it is essential to know the spin-polarization of these materials. However, the methods for analysing it are still rare.

Positron annihilation spectroscopy (PAS) experiment attracted much attentions for its powerful application for detecting electronic structure especially the vacancy defect in materials.

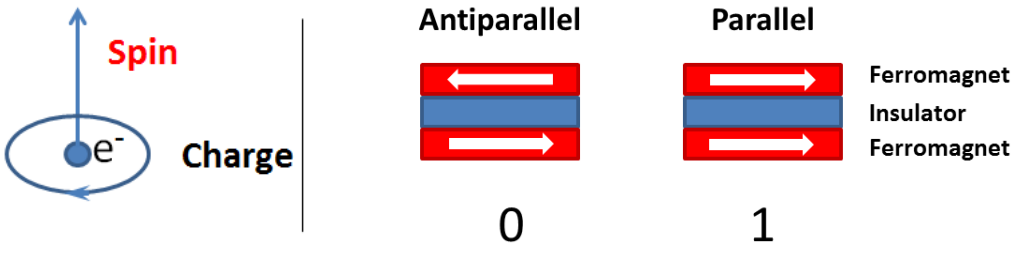

(a) electron (b) spintronics for data storage

Figure 1.2: Spin of elecron and its application.

And the advantage of this PAS tool is not only the ability to detect point defect, but also the harmless to the structure of materials.

Then, spin-polarized positron annihilation spectroscopy (SP-PAS) experiment is expected to detect spin-polarization or further information of electrons in materials. This is because when a positron goes into a sample like the bulk metal (Fig.1.3.a), the positron which is the antiparticle of electron can contact electron, then annihilate and give out photons. By detecting the photons, it is possible to know the information of electrons. Here, the two photon case (main annihilation case) that the electron and the positron have different spin directions is show in Fig.1.3.a. If the electron and the positron have no kinetic energy, each of the two photons has energy of 511 eV which can obtain from the mass-energy equivalence.

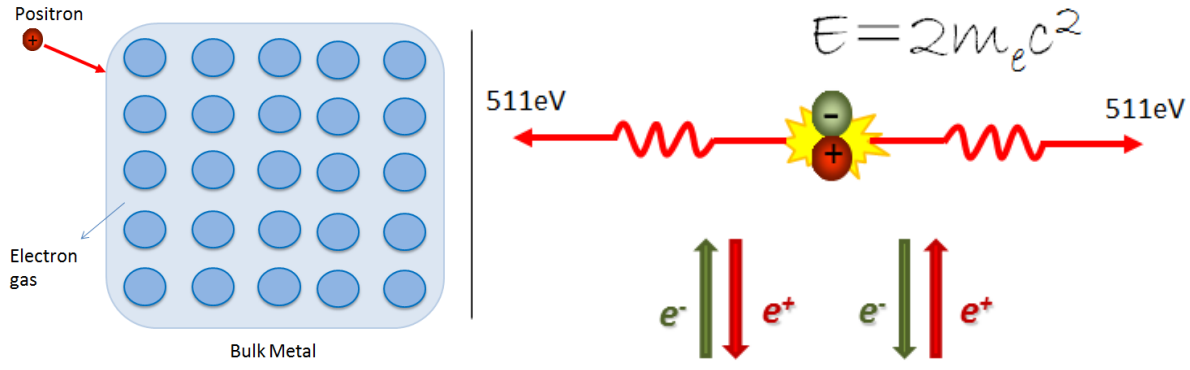

(a) (b)

Figure 1.3: Positron annihilation in bulk metal.

There are few previous experimental studies. The 3γ spin-polarized positron experiment on ferromagnetic materials was first carried out by S.Berko in 1971[37]. Later, two-dimensional two-photon angular correlation of the spin-polarized positron annihilation radiation in Ni[38, 39, 40] and Co[41], and the Doppler broadening of annihilation radiation[34, 35] were measured. These experiments allow us to get information on the spin polarization in ferromagnetic materials. Then, it is expected that positron annihilation experiment can be applied to study spintronics. However, theoretical study is necessary to analyze the experimental results.

1.4 Structure of The Thesis

In this thesis, the theories and methods are mentioned in the Chapter 2. In Chapter 3, we report our results related to the first topics which is the study of the calculations of formation energy and healing barriers of adatom-vacancy pair defect. We will discuss the stability of the defect geometries, magnetic property, and the healing behaviour of the adatom-vacancy pair defect. In Chapter 4, the second topics of our study is demonstrated. The results of spin-polarized positron lifetime calculations will be reported. We will confirm the reliability of our simulation scheme and discuss the results with experimental results. Then, I summarize our work and future scope in Chapter 5. In the final part, I would like to express my thanks in Acknowledgements.

Chapter 2

Theory and Calculational Details

THe results in this dissertation are obtained by using the first-principles quantum-mechanical calculations. In the first-principles calculations, no empirical parameters are employed in simulations to compute the electronic properties of a system, but only the atomic numbers and positions are used in calculations. Due to an increase in processing power of the computer in the past few decades, it is possible to perform first-principles calculations on a larger and more realistic systems. The calculations acquire a degree of accuracy, which enables direct comparison to experiments.

In this chapter, a brief overview of the theoretical methods is explained. We use the PHASE [2] calculation code. The PHASE is based on density functional theories (DFT), pseudopotentials, and plane wave basis set. We explain the theoretical background in section 2.1. In section 2.2 density functional theory is denoted. The exchange and correlation functionals, plane wave methods, and pseodopotentials are described in sections 2.3, 2.4 and 2.5, respectively. We explain calculational details in section 2.8.

2.1 Theoretical Background

The Hamiltonian of a fully interacting system consisting of many electrons and nuclei is expressed as:

$$\hat{H} = \hat{T_e} + \hat{T_n} + \hat{V_{ee}} + \hat{V_{nn}} + \hat{V_{ext}} \tag{2.1}$$

where $\hat{T_e}$, $\hat{T_n}$, $\hat{V_{ee}}$, $\hat{V_{nn}}$, and $\hat{V_{ext}}$ are the many electron kinetic energy operator, many-nucleus kinetic energy operator, the electron-electron interaction energy operator, many-nucleus kinetic energy operator,and the electron-nucleus interaction energy operator, respectively.

They are expressed as following:

$$\begin{cases} \hat{T_e} = -\frac{1}{2}\sum_i^N \nabla_i^2(r_i) \\ \hat{T_n} = -\frac{1}{2}\sum_j \frac{1}{M_j}\nabla_j^2(\mathbf{R}_j) \\ \hat{V_{ee}} = \frac{1}{2}\sum_{i\neq j} \frac{1}{|\mathbf{r}_i - \mathbf{r}_j|} \\ \hat{V_{nn}} = \frac{1}{2}\sum_{i\neq j} \frac{Z_i Z_j}{|\mathbf{R}_i - \mathbf{R}_j|} \\ \hat{V_{ext}} = -\sum_{i,j} \frac{Z_j}{|\mathbf{R}_i - \mathbf{R}_j|} \end{cases} \tag{2.2}$$

where the r_i is the position of the electron i, and the M_j, Z_j, and $\mathbf{R}_j$ are the mass, atomic number and position of the nucleus j respectively.

The Schrödinger eigenvalue equation of this system is given by:

$$\hat{H}\Psi = E\Psi, \tag{2.3}$$

where the system wavefunction Ψ depends on all configuration variable which is expresses as:

$$\Psi = \Psi(\mathbf{r_1}, \mathbf{R_1}, \mathbf{r_2}, \mathbf{R_2}, ...). \tag{2.4}$$

This equation is defined in $3M + 3N$-parameter space, and it is too complex that impossible to solve for all but the simplest systems.

Considering the mass of a nucleus is much larger than that of an electron, we can assume that the motion of the nuclei is negligible compared to that of the electrons and fix their positions. By employing this, we can neglect $\hat{T_n}$ and $\hat{V_{nn}}$ and rewrite it as a problem of many electrons in an external potential $\hat{V_{ext}}$ generated by the stationary nuclei:

$$\hat{H} = \hat{T} + \hat{V_{ee}} + \hat{V_{ext}}, \tag{2.5}$$

The Schrödinger equation of this system is expressed as:

$$\hat{H}\Psi = \left[-\frac{1}{2}\sum_{i}^{N} \nabla^2 + \frac{1}{2}\sum_{i \neq j} \frac{1}{|\mathbf{r}_i - \mathbf{r}_j|} - \sum_{i,j} \frac{Z_j}{|\mathbf{R}_i - \mathbf{R}_j|} \right] \Psi = E\Psi, \tag{2.6}$$

with Ψ now the many-electron wavefunction,

$$\Psi = \Psi(\mathbf{r_1}, \mathbf{r_2}, ...). \tag{2.7}$$

This approximation method is called the **Born-Oppenheimer approximation** and is employed in all systems that are more complex than the hydrogen atom.

We know that it is possible to find the total ground state solution if we are capable of finding the ground state solutions for fixed nuclear configurations, but it is still necessary to reduce the efforts of finding the total ground state solution. For this, it is useful to introduce some additional approximations, such as variation principle and Hartree-Fock approximation. Before we explain Hartree-Fock approximation, first we discuss the variation principle.

2.1.1 Variation Principle

To find any eigenfunction of the Hamiltonian operator is an impossible task, but we may consider all the (many-body) eigenfunctions ϕ_i were known. Assuming that the set of these eigenfunctions is complete, we may expand any other wavefunctions ψ of the system with the same number of electrons. We, therefore, write down the following expansion.

$$|\Psi\rangle = \sum_i c_i |\phi_i\rangle \tag{2.8}$$

where c_i are the expansion coefficients. The eigenstates $|\phi_i\rangle$ are assumed to be orthonormal. The wavefuntion is assume to be normalized, then the expectation value for the energy of the wavefunction is given by:

$$E = \langle\Psi|\hat{H}|\Psi\rangle = \sum_{i,j} c_j^* c_i \langle\phi_i|\hat{H}|\phi_j\rangle = \sum_i |c_i^2| E_i \geq E_0 \sum_i |c_i^2| = E_0 \tag{2.9}$$

with E_0 the lowest eigenvalue of $\hat{H}$, i.e. the ground state energy. The expectation value of the energy of any wavefunction ψ is thus higher than or equal to the ground state energy. This result is very important since it allows us to search for the ground state by testing different 'trial wavefunctions'.

Now the problem is to find out a good trial wavefunctions. In practice, the approximate wavefunction is written in terms of one or more parameters:

$$\Psi = \Psi(p_1, p_2, ..., p_N) \tag{2.10}$$

So, the expectation value for the energy, E, is a function of these parameters and can be minimized with respect to them by requiring that

$$\frac{\partial E(p_1, p_2, ..., p_N)}{\partial p_1} = \frac{\partial E(p_1, p_2, ..., p_N)}{\partial p_2} = ... = \frac{\partial E(p_1, p_2, ..., p_N)}{\partial p_n} = 0 \tag{2.11}$$

Let us assume that the approximate wavefunction for a given system may be expanded in terms of a particular set of plane waves. Because we cannot work with an infinitely many numbers of plane waves, we truncate the sum and just consider the first N terms:

$$\phi = \sum_{j}^{N} c_j \exp(-i\mathbf{k} \cdot \mathbf{r_j}) \tag{2.12}$$

In order to get a good approximation ground state, we would like the above expansion to satisfy the minimum condition, i.e:

$$\frac{\partial}{\partial c_j^*} \frac{\langle \phi | \hat{H} | \phi \rangle}{\langle \phi | \phi \rangle} = 0 \tag{2.13}$$

for each c_j. In addition, we require the approximate wavefunction to remain normalized:

$$\langle \phi | \phi \rangle = 1 \tag{2.14}$$

which then we can rewrite Eq.(2.13) as:

$$\frac{\partial}{\partial c_j^*} \langle \phi | \hat{H} | \phi \rangle = 0 \tag{2.15}$$

for all c_j. We can satisfy Eq.(2.14) and Eq.(2.15) by introducing a new quantity which is expressed as:

$$K = \langle \phi | \hat{H} | \phi \rangle - \lambda \left[\langle \phi | \phi \rangle - 1 \right] \tag{2.16}$$

and extending the minimization property to include extra parameter λ,

$$\frac{\partial K}{\partial c_j^*} = \frac{\partial K}{\partial \lambda} = 0. \tag{2.17}$$

Here λ is called the *Lagrange multipliers*. Inserting the expansion in Eq.(2.12) into Eq.(2.17), we get

$$\sum_j c_j \left(\langle exp(-i\mathbf{k}\cdot\mathbf{r_i})|\hat{H}|exp(-i\mathbf{k}\cdot\mathbf{r_j})\rangle - \lambda\langle exp(-i\mathbf{k}\cdot\mathbf{r_i})|exp(-i\mathbf{k}\cdot\mathbf{r_j})\rangle \right) = 0 \tag{2.18}$$

We can write in the form of a generalized eigenvalue equation,

$$\sum_j H_{ij}c_j = \lambda\delta_{ij} \tag{2.19}$$

where $H_{ij} = \langle exp(-i\mathbf{k}\cdot\mathbf{r_i})|\hat{H}|exp(-i\mathbf{k}\cdot\mathbf{r_j})\rangle$ and $\delta_{ij} = \langle exp(-i\mathbf{k}\cdot\mathbf{r_i})|exp(-i\mathbf{k}\cdot\mathbf{r_j})\rangle$. We can solve these N equations ($i = 1, 2, ...N$) by calculating the matrix element H_{kj} and δ_{ij}. If we use N basis functions to expand the trial function ϕ, Eq.(2.12) then gives N eigenvalues. By multiplying Eq.(2.18) with c_i^* and summing over i we get the following expression;

$$\lambda = \frac{\sum_{i,j} c_i^* c_j \langle exp(-i\mathbf{k}\cdot\mathbf{r_i})|\hat{H}|exp(-i\mathbf{k}\cdot\mathbf{r_j})\rangle}{\sum_{i,j} c_i^* c_j \langle exp(-i\mathbf{k}\cdot\mathbf{r_i})|exp(-i\mathbf{k}\cdot\mathbf{r_j})\rangle} \tag{2.20}$$

Eq. (2.20) implies that each of the N eigenvectors correspond to a series of expansion coefficients yielding different ϕ and each λ corresponds to a different expectation value. The eigenvector corresponds to the smallest eigenvalue then corresponds to the best ϕ and the smallest eigenvalue itself is the closest approximation to the ground state energy.

2.1.2 Hartree-Fock Approximation

A major problem with trying to solve the many-body Schrödinger equation is the representation of the many-body wavefunction. In 1920, Douglas Hartree [3] developed an approach named after himself called the Hartree approximation. He simplified the problem of electron-electron interactions by assuming that the many-electron wavefunction is expressed as a product of single electron wavefunction which is capable of solving the multi-electron Schrödinger equation

of the wavefunction. With this hypothesis and the use of the **variation principle**, we need to solve N equations for an N single electrons system,

$$\Psi_H(\mathbf{r_1}, \mathbf{r_2}, \mathbf{r_3}, ...\mathbf{r_N}) = \frac{1}{\sqrt{N}}\phi(\mathbf{r_1}), \phi(\mathbf{r_2}), \phi(\mathbf{r_3}), ...\phi(\mathbf{r_N}) \tag{2.21}$$

where $\Psi(\mathbf{r_i})$ consists of one-electron wavefunction $\phi(\mathbf{r_i})$.

However, the Hartree approximation does not account for exchange interaction as Eq.(2.21) does not satisfy **Pauli's exclusion principle**. According to **Pauli's exclusion principle** it is known that Hartree approximation fails as the Hartree product wavefunction is symmetric not antisymmetric.

We need to establish does not satisfy the Pauli's exchange principle. Hartree and Fock introduce an approximation method that deals with electrons as distinguishable particle. In the Hartree-Fock scheme, the system with N-electron wave function is approximated by *antisymmetric* function.

The Hartree-Fock scheme is always described as *Slater Determinant* such as:

$$\Psi_{HF} = \frac{1}{\sqrt{N!}} \begin{vmatrix} \phi_1(\mathbf{r_1}) & \phi_2(\mathbf{r_1}) & \cdots & \phi_{N/2}(\mathbf{r_1}) \\ \phi_1(\mathbf{r_2}) & \phi_2(\mathbf{r_2}) & \cdots & \phi_{N/2}(\mathbf{r_2}) \\ \vdots & \vdots & \cdots & \vdots \\ \phi_1(\mathbf{r_N}) & \phi_2(\mathbf{r_N}) & \cdots & \phi_{N/2}(\mathbf{r_N}) \end{vmatrix} \tag{2.22}$$

or in short:

$$\Psi_{HF} = \frac{1}{\sqrt{N!}} det\left|(\mathbf{r_1})\phi_2(\mathbf{r_2}).....\phi_{N/2}(\mathbf{r_N})\right| \tag{2.23}$$

with additional orthonormal constraint

$$\int \phi_i^*(\mathbf{r})\phi_i(\mathbf{r})d\mathbf{r} = \langle\phi_i|\phi_j\rangle = \delta_{ij} \tag{2.24}$$

With the above Slater Determinant, we can be determined the HF energy by taking the expectation value of the Hamitonian Eq.(2.6). It can be expressed by the given equation:

$$E = \langle\Psi_{HF}|\hat{H}|\Psi_{HF}\rangle = 2\sum_{i}^{N/2} h_i + \sum_{i}^{N/2}\sum_{j}^{N/2}(2J_{i,j} - K_{i,j}) \tag{2.25}$$

the first term of the Eq. (2.25) indicates the kinetic energy of electrons and interaction between electrons-nuclei, then the second term represents the interaction between two electrons called Coulomb and exchange integrals, where: where

$$h_i = \int \phi_i^*(\mathbf{r_1})\hat{h}\phi_i(\mathbf{r_1})d\mathbf{r_1} \tag{2.26}$$

$$\mathbf{J_{ij}} = \int\int \phi_i^*(\mathbf{r_1})\phi_i(\mathbf{r_1})\frac{1}{|\mathbf{r_1}-\mathbf{r_2}|}\phi_j^*(\mathbf{r_2})\phi_j(\mathbf{r_2})d\mathbf{r_1}d\mathbf{r_2} \tag{2.27}$$

$$\mathbf{K_{ij}} = \int\int \phi_i^*(\mathbf{r_1})\phi_j(\mathbf{r_1})\frac{1}{|\mathbf{r_1}-\mathbf{r_2}|}\phi_j^*(\mathbf{r_2})\phi_i(\mathbf{r_2})d\mathbf{r_1}d\mathbf{r_2} \tag{2.28}$$

The term $\mathbf{J_{ij}}$ are called Coulomb integrals, which are already present in the Hartree Approximation. On the other hand, the exchange integral $\mathbf{K_{ij}}$ are represented something new. It is not necessary to exclude the term $i = j$ because $J_{ij} = K_{ij}$.

In order to understand Coulomb and exchange interaction in Eq. 2.25, we consider V_{HF} as Hartree-Fock potential. This potential describes the repulsive interaction between one electron with others N-1 electrons averagely, consists Coulomb operator $\hat{J}$ and exchange operator $\hat{K}$.

$$\hat{J}\phi(\mathbf{r}) = \int d\mathbf{r_2}\frac{|\phi_j(\mathbf{r_2})|^2}{|\mathbf{r_1}-\mathbf{r_2}|}\phi_i(\mathbf{r_1}) \tag{2.29}$$

$$\hat{K}\phi(\mathbf{r}) = \int d\mathbf{r_2}\frac{\phi_j^*(\mathbf{r_2})\phi_i(\mathbf{r_2})}{|\mathbf{r_1}-\mathbf{r_2}|}\phi_j(\mathbf{r_1}) \tag{2.30}$$

The Hartree-Fock theory neglect the electronic correlation. Therefore, the ground-state energy calculated from the Hartree-Fock theory is always higher than the true ground-state energy ($E_{HF} > E_0$).

The Hartree-Fock scheme is constructed based on the effective wavefunction and potential. We guess the first set input of Slater determinant based on Pauli's principle for the system, so we have reasonable approximation wave function. Then we construct the potential operator with emphasizing the electron's interaction that taken account averagely and considering the self-interaction in one electron. Next iteration is done based on the new orbitals from previous

calculation until we reach the threshold point. This technique is also known as *self-consistent field* (SCF).

2.2 Density Functional Theory (DFT)

The Hartree-Fock equations deal with exchange exactly; however, the equations neglect correlations due to many-body interactions. However, the effects of electronic correlations are not negligible. The requirement for a computationally practicable scheme successfully incorporates the effects of both exchange and correlation, and it leads us to consider the conceptually disarmingly simple and elegant density functional theory(DFT). Nowadays, DFT is an efficient and practical method to describe ground state properties of materials due to high computational efficiency and good accuracy. The idea of DFT is to describe interacting system via electron's density, not wave functions. DFT is totally based on two theorems stated by Hohenberg and Kohn [4]. Here we explain the two theorems as following:

2.2.1 Hohenberg-Kohn Theorems

There are two important theorems that can be resumed from Hohenberg-Kohn work. The theorems support us for determining the Hamiltonian operator, and the properties of the system based on electron density point of view. The electronic density $n(\mathbf{r})$ is expressed as:

$$n(\mathbf{r}) = \mathbf{N} \sum_{\mathbf{s_1}} ... \sum_{\mathbf{s_N}} \int ... \int |\mathbf{\Psi}(\mathbf{r}, \mathbf{s_1}, \mathbf{r_2}, \mathbf{s_2}, ...\mathbf{r_N}, \mathbf{s_N})|^{\mathbf{2}} \mathbf{dr_2}.....\mathbf{dr_N} \tag{2.31}$$

$$\int n(\mathbf{r}) d\mathbf{r} = N \tag{2.32}$$

Theorem I. (Hohenberg-Kohn 1, 1964) *The ground state density $n(\mathbf{r})$ of a many-body quantum system in some external potential $V_{ext}(\mathbf{r})$ determines this potential uniquely.*

Proof: Hohenberg-Kohn proved the first theorem by *reducio ad absurdum*. They assumed another external potential, $V'_{ext}(\mathbf{r})$, that differed by a constant from first external potential but give rise to the same density $n(\mathbf{r})$. Now, we have two Hamiltonian operator, $\hat{H}$ and $\hat{H}'$, that give corresponding ground wave function (Ψ and Ψ') and energies (E_0 and E'_0). Obviously;

these two ground state energies are different. This condition gives us a chance to use the Ψ' for calculating the expectation value of $\hat{H}$:

$$E_0 < \langle \Psi' | \hat{H} | \Psi' \rangle = \langle \Psi' | \hat{H}' | \Psi' \rangle + \langle \Psi' | \hat{H} - \hat{H}' | \Psi' \rangle \tag{2.33}$$

As the value of Hamiltonian are: $\hat{H} = \hat{T} + \hat{V}_{ee} + \hat{V}_{ext}$ and $\hat{H} = \hat{T} + \hat{V}_{ee} + \hat{V}'_{ext}$. We can get:

$$E_0 < E'_0 + \int n(\mathbf{r})[V_{ext} - V'_{ext}]d\mathbf{r} \tag{2.34}$$

and (by changing the quantities)

$$E'_0 < E_0 + \int n(\mathbf{r})[V_{ext} - V'_{ext}]d\mathbf{r} \tag{2.35}$$

Then we add the Eq. (2.34) and Eq. (2.35), this summation will lead to inconsistency:

$$E_0 + E'_0 < E_0 + E'_0 \tag{2.36}$$

Thus the theorem proved by *reductio ad absurdum*

Theorem II. (Hohenberg-Kohn 2, 1964) *A universal functional for the energy $E[n]$ in terms of the density $n(\mathbf{r})$ can be defined, valid for any external potential $V_{ext}(\mathbf{r})$. For any particular $V_{ext}(\mathbf{r})$, the exact ground state energy of the system is the global minimum value of this functional, and the density $n(\mathbf{r})$ that minimizes the functional is the exact ground state density $n_0(\mathbf{r})$.*

Proof: Since all properties such as the kinetic energy, etc., are uniquely determined if $n(\mathbf{r})$ is specified, then each such property can be viewed as a functional of $n(\mathbf{r})$, including the total energy functional:

$$\begin{aligned} E_{HK}[n(\mathbf{r})] &= T[n] + E_{int}[n] + \int v_{ext}(\mathbf{r}) n(\mathbf{r}) d^3\mathbf{r} + E_{II} \\ &= F[n(\mathbf{r})] + \int v_{ext}(\mathbf{r}) n(\mathbf{r}) d^3\mathbf{r} + E_{II} \end{aligned} \tag{2.37}$$

where E_{II} is the interaction energy of nuclei and $F[n(\mathbf{r})]$ is a universal functional of the charge density $n(\mathbf{r})$ because the treatment of the kinetic and internal potential energies are the same for all systems. In the ground state, the energy is defined by the unique ground state density, $n^{(1)}(\mathbf{r})$,

$$E_0 = E[n^{(1)}] = \langle \Psi | \hat{H} | \Psi \rangle \tag{2.38}$$

By the variational principle, a different density, $n^{(2)}\mathbf{r})$ will necessarily give a higher energy:

$$E_0 = E[n^{(1)}] = \langle\Psi|\hat{H}|\Psi\rangle < \langle\Psi'|\hat{H}|\Psi'\rangle = E_0^{'} \tag{2.39}$$

It follows that minimizing with respect to $n(\mathbf{r})$ the total energy of the system written as a functional of $n(\mathbf{r})$, one finds the total energy of the ground state. The correct density that minimizes the energy is then the ground state density. In this way, DFT exactly reduce the N-body problem to the determination of a 3-dimensional function $n(\mathbf{r})$ which minimize the functional $E_{HK}[n(\mathbf{r})]$. But unfortunately this is of little use as $E_{HK}[n(\mathbf{r})]$ is not known.

2.2.2 Kohn-Sham equations

Kohn-Sham reformulated the problem in a more familiar form and opened the way to practical applications of DFT. They continued to prove the theorem which states that the total energy of the system depends only on the electron density of the system [5].

$$E = E[n(\mathbf{r})] \tag{2.40}$$

An interacting electrons system is mapped in an auxiliary system of a non-interacting electrons with the same ground state charge density $n(r)$.For a system of non-interacting electrons the ground-state charge density is represented as a sum over one-electron orbitals.

$$n(\mathbf{r}) = 2\sum_{i}^{N} |\Psi_i(\mathbf{r})|^2, \tag{2.41}$$

where i runs from 1 to $N/2$ if we consider double occupancy of all states.

The electron density n(**r**) can be varied by changing the wave function $\Psi(\mathbf{r})$ of the system. If the electron density n(**r**) corresponds to the said wavefunction, then its total energy is the minimized energy, and the whole system is in a ground state. The Kohn-Sham approach is to replace interacting electron, which is difficult with non-interacting electrons, which move in an effective potential [5]. The effective potential consists the external potential, and Coulomb interaction between electrons, and its effect such as exchange and correlation interactions. By solving the equations, we can get ground state density and energy. The accuracy of the solution

is limited to the approximation of exchange and correlation interactions. It is convenient to write Kohn-Sham energy functional for the ground state including external potential is:

$$E_{KS} = T_s[n(\mathbf{r})] + E_H[n(\mathbf{r})] + E_{XC}[n(\mathbf{r})] + \int d\mathbf{r} V_{ext}(\mathbf{r}) n(\mathbf{r}) \tag{2.42}$$

The first term is the kinetic energy of non-interacting electrons:

$$T_s[n(\mathbf{r})] = -\frac{\hbar^2}{2m} 2 \sum_i \int \Psi_i^*(\mathbf{r}) \nabla^2 \Psi_i^*(\mathbf{r}) d\mathbf{r} \tag{2.43}$$

The second term (called the Hartree energy) contains the electrostatic interaction between cloud of charge:

$$E_H[n(\mathbf{r})] = \frac{e^2}{2} \int \frac{n(\mathbf{r}) n(\mathbf{r}')}{|\mathbf{r} - \mathbf{r}'|} d\mathbf{r} d\mathbf{r}' \tag{2.44}$$

All effects of exchange and correlation are grouped into exchange-correlation energy E_{XC}. If all the functional $E_{XC}[n(\mathbf{r})]$ were known, we could obtain exact ground state density and energy of the many body problem.

Kohn-Sham energy problem is a minimization problem with respect of the density $n(\mathbf{r})$. Solution of this problem can be obtained by using functional derivative as below

$$\begin{aligned} \frac{\delta E_{KS}}{\delta \Psi_i^*(\mathbf{r})} = & \frac{\delta T[n]}{\delta \Psi_i^*(\mathbf{r})} + \left[\frac{\delta E_{ext}[n]}{\delta n(\mathbf{r})} + \frac{\delta E_H[n]}{\delta n(\mathbf{r})} + \frac{\delta E_{XC}[n]}{\delta n(\mathbf{r})} \right] \frac{\delta n(\mathbf{r})}{\delta \Psi_i^*(\mathbf{r})} \\ & - \frac{\delta \left(\lambda \left(\int n(\mathbf{r}) d\mathbf{r} - N \right) \right)}{\delta n(\mathbf{r})} \left[\frac{\delta n(\mathbf{r})}{\delta \Psi_i^*(\mathbf{r})} \right] = 0, \end{aligned} \tag{2.45}$$

where λ is Lagrange multiplier and The exchange-correlation potential, V_{XC}, is given formally by the functional derivative

$$V_{XC} = \frac{\delta E_{XC}[n]}{\delta n(\mathbf{r})} \tag{2.46}$$

$$\frac{\delta n(\mathbf{r})}{\delta \Psi_i^*(\mathbf{r})} = \Psi_i(\mathbf{r}),$$

the last term is Lagrange multiplier for handling the constraints, so we can get non-trivial solution.

The first, second, and third terms of eq. (2.45) are

$$\frac{\delta T[n]}{\delta \Psi_i^*(\mathbf{r})} = -\frac{\hbar^2}{2m} 2\nabla^2 \Psi_i(\mathbf{r}) \tag{2.47}$$

$$\left[\frac{\delta E_{ext}[n]}{\delta n(\mathbf{r})} + \frac{\delta E_H[n]}{\delta n(\mathbf{r})} + \frac{\delta E_{XC}[n]}{\delta n(\mathbf{r})}\right] \frac{\delta n(\mathbf{r})}{\delta \Psi_i^*(\mathbf{r})} = 2(V_{ext}(\mathbf{r}) + V_H(\mathbf{r}) + V_{XC}(\mathbf{r}))\Psi_i(\mathbf{r}),$$
$$\frac{\delta\left(\lambda\left(\int n(\mathbf{r})d\mathbf{r} - N\right)\right)}{\delta n(\mathbf{r})}\left[\frac{\delta n(\mathbf{r})}{\delta \Psi_i^*(\mathbf{r})}\right] = 2\varepsilon_i \Psi_i(\mathbf{r}) \tag{2.48}$$

Inserting eq. (2.47), and (2.48) to eq. (2.45), we can obtain Kohn-Sham equation which satisfies many body Schrödinger equation.

$$\left(-\frac{1}{2}\nabla^2 + V_{KS}(\mathbf{r})\right)\Psi_i(\mathbf{r}) = \varepsilon_i \Psi_i(\mathbf{r}) \tag{2.49}$$

where

$$V_{KS}(\mathbf{r}) = V_{ext}(\mathbf{r}) + V_H(\mathbf{r}) + V_{XC}(\mathbf{r}) \tag{2.50}$$

or,

$$V_{KS}(\mathbf{r}) = V_{ext}(\mathbf{r}) + \frac{e^2}{2}\int \frac{n(\mathbf{r}')}{|\mathbf{r} - \mathbf{r}'|} d\mathbf{r}' + V_{XC}(\mathbf{r}) \tag{2.51}$$

If the virtual independent-particle system has the same ground state as the real interacting system, then the many-electron problem reduces to one electron problem. Thus we can write:

$$V_{KS}(\mathbf{r}) = V_{eff}(\mathbf{r}) \tag{2.52}$$

The kinetic energy $T_s[n(\mathbf{r})]$ is given by

$$T_s[n(\mathbf{r})] = \sum_i \varepsilon_i - \int n(\mathbf{r}) V_{eff}(\mathbf{r}) d\mathbf{r} \tag{2.53}$$

By substituting this formula in equation 2.42, the total energy is given by as follows:

$$E_{KS}[n(\mathbf{r})] = \sum_i \varepsilon_i + \frac{1}{2}\int\int \frac{n(\mathbf{r})n(\mathbf{r}')}{|\mathbf{r} - \mathbf{r}'|} d\mathbf{r} d\mathbf{r}' + E_{xc}[n] - \int n(\mathbf{r}) V_{eff}(\mathbf{r})) d\mathbf{r} \tag{2.54}$$

Since the Hartree term and V_{xc} depend on $n(\mathbf{r})$, which depend on Ψ_i, the problem of solving the Kohn-Sham equation has to be done in a self-consistent (iterative) way. Usually one starts

with an initial guess for $n(\mathbf{r})$, then calculates the corresponding V_H and V_{xc} solves the Kohn-Sham equations for the Ψ_i . From this one calculates a new density and starts again. This procedure is then repeated until convergence is reached (Fig. **??**)

2.3 Exchange and Correlation Functional

The major problem with DFT is that the exact functionals for exchange and correlation are not known except for the free-electron gas. In previous section, the many body problems are rewritten to the effective one-electron problem by using the Kohn-Sham equation. But, the Kohn-Sham equation cannot be solved since the derivative $E_{XC}[n(\mathbf{r})]$ is not known. Therefore, it is very important to have an accurate XC energy functional $E_{XC}[n(\mathbf{r})]$ or potential $V_{XC}(\mathbf{r})$ in order to give a satisfactory description of a realistic condensed-matter system. For a homogeneous electron gas, this will only depend on the value of the electron density. For a non-homogeneous system, the value of the exchange correlation potential at the point $\mathbf{r}$ depend not only on the value of density at $\mathbf{r}$, but also the variation close to $\mathbf{r}$.

2.3.1 Local Density Approximation (LDA)

As the functional $E_{XC}[n(\mathbf{r})]$ is unknown one has to find a good approximation for it. A simple approximation, which was already suggested by Hohenberg and Kohn, is the LDA or in the spin polarized case the local-spin-density approximation (LSDA). The exchange-correlation energy per particle by its homogeneous electron gas (HEG) $e_{XC}[n(\mathbf{r})]$ is expressed by:

$$\begin{aligned} E_{xc}^{LDA}[n(\mathbf{r})] &= \int n(\mathbf{r}) e_{xc}^{homo}(n(\mathbf{r}))d\mathbf{r} \\ &= \int n(\mathbf{r}) \left[e_x^{homo}(n(\mathbf{r})) + e_c^{homo}(n(\mathbf{r}))\right] d\mathbf{r} \end{aligned} \tag{2.55}$$

for spin polarized system

$$E_{xc}^{LSDA}[n_+(\mathbf{r}), n_-(\mathbf{r})] = \int n(\mathbf{r}) e_{xc}^{homo}(n_+(\mathbf{r}), (n_-(\mathbf{r}))d\mathbf{r} \tag{2.56}$$

The exchange energy $e_x(n(\mathbf{r}))$ is

$$e_x^{LDA}(n(\mathbf{r})) = -\frac{3}{4\pi} k_f \tag{2.57}$$

where the Fermi wavevector $k_f = (3\pi^2 n)^{\frac{1}{3}}$.

The expression of the correlation energy density of the HEG at high density limit has the form:

$$e_c = Aln(r_s) + B + r_s(Cln(r_s) + D) \tag{2.58}$$

and the density limit takes the form

$$e_c = \frac{1}{2}\left(\frac{g_0}{r_s} + \frac{g_1}{r_s^{3/2}} + ...\right) \tag{2.59}$$

where where the Wigner-Seitz radius r_s is related to the density as

$$r_s = (3/(4\pi n))^{\frac{1}{3}} \tag{2.60}$$

For spin polarized systems, the exchange energy functional is known exactly from the result of spin-unpolarized functional:

$$E_x[n_+(\mathbf{r}), n_-(\mathbf{r})] = \frac{1}{2}(E_x[2n_+(\mathbf{r})] + E_x[2n_-(\mathbf{r})]) \tag{2.61}$$

The spin-dependence of the correlation energy density is approached by the relative spin-polarization:

$$\xi(\mathbf{r}) = \frac{n_+(\mathbf{r}) - n_-(\mathbf{r})}{n_+(\mathbf{r})n_-(\mathbf{r})} \tag{2.62}$$

The spin correlation energy density $e_c(n(\mathbf{r}), \xi(\mathbf{r})$ is so constructed to interpolate extreme values $\xi = 0, \pm 1$, corresponding to spin-unpolarized and ferromagnetic situations. The XC potential $V_{XC}(n(\mathbf{r}))$ in LDA is given by:

$$\frac{\delta E_{XC}[n]}{\delta n(\mathbf{r})} = \int d\mathbf{r}\left[\epsilon_{xc} + n\frac{\partial \epsilon_{xc}}{\partial n}\right] \tag{2.63}$$

$$V_{XC}(\mathbf{r}) = \epsilon_{xc} + n\frac{\partial \epsilon_{xc}}{\partial n}, \tag{2.64}$$

$$E_{XC}[n] = \int d\mathbf{r} n(\mathbf{r})\epsilon_{xc}([n], \mathbf{r}), \tag{2.65}$$

where $\epsilon_{xc}([n], \mathbf{r})$ is the energy per electron that depends only on the density $n(\mathbf{r})$.

The LDA sometimes allows useful predictions of electron densities, atomic positions, and vibration frequencies. However, The LDA also makes some errors: total energies of atoms are less realistic than those of HF approximation, and binding energies are overestimated. LDA also systematically underestimates the band gap.

2.3.2 Generalized Gradient Approximation (GGA)

The density of electron is not always homogeneous as we expected. In the case of inhomogeneous density, naturally, we have to carry out the expansion of electronic density in the term of gradient and higher order derivatives, and they are usually termed as generalized gradient approximation (GGA). GGAs are still local but also take into account the gradient of the density at the same coordinate. Three most widely used GGAs are the forms proposed by Becke [6] (B88) , Perdew et al. [7, 8], and Perdew, Burke and Enzerhof [9] (PBE). The definition of the exchange-correlation energy functional of GGA is the generalized form in Eq. (2.56)to include corrections from density gradient $\nabla n(\mathbf{r})$ as :

$$E_{xc}^{GGA}[n_+(\mathbf{r}), n_-(\mathbf{r})] = \int n(\mathbf{r}) e_{xc}[n(\mathbf{r}) F_{XC}[n(\mathbf{r}), |\nabla n_+(\mathbf{r})|, |\nabla n_-(\mathbf{r})|, ...] d\mathbf{r} \tag{2.66}$$

Here, F_{XC} is the escalation factor that modifies the local density approximation (LDA) expression according to the variation of density in the vicinity of the considered point, and it is dimensionless [10]. The exchange energy expansion will introduce a term that proportional to the squared gradient of the density. If we considered up to fourth order, the similar term also appears proportional to the square of the density's Laplacian. Recently, the general derivation of the exchange gradient expansion has been up to sixth order by using second order density response theory [11]. The lowest order (fourth order) terms in the expansion of F_x have been calculated analytically [11, 12]. This term is given by the following:

$$F_X(m, n) = 1 + \frac{10}{81} m + \frac{146}{2025} m^2 - \frac{73}{405} nm + Dm^2 + O(\nabla\rho^6) \tag{2.67}$$

where

$$m = \frac{|\nabla\rho|^2}{4(3\pi^2)^{2/3}\rho^{8/3}} \tag{2.68}$$

is the square of the reduced density gradient, and

$$n = \frac{\nabla^2\rho}{4(3\pi^2)^{2/3}\rho^{5/3}} \tag{2.69}$$

is the reduced Laplacian of density.

These are the comparison of GGAs with LDA (LSDA)

1. It enhances the binding energies and atomic energies,

2. It enhances the bond length and bond angles,

3. It enhances the energetics, geometries, and dynamical properties of water, ice, and water clusters,

4. Semiconductors are marginally better described within the LDA than in GGA, except for binding energies,

5. For *4d-5d* transition metals, the improvement of GGA over LDA is not clear, depends on how well the LDA does in each particular case,

6. Lattice constant of noble metals (Ag, Au, and Pt) are overestimated in GGA, and

7. There is some improvement in the gap energy; however, it is not substantial as this feature related to the description of the screening of the exchange hole when one electron is removed, and this point is not taken into account by GGA.

2.4 Plane Waves Method

The plane wave method is much more efficient than all-electron ones to calculate the atomic forces and hence to determine the equilibrium geometries. Plane waves are not centered at the nuclei but extend throughout the complete space. They implicitly involve the concept of periodic boundary condition. Therefore, they enjoy great popularity in solid state physics for which they are particularly adopted. The Kohn-Sham equation can be described by using plane waves. As the arrangement of the atoms within the cell is periodic in the real space, so the wave functions must satisfy Bloch's theorem, which can be written by:

$$\Psi_i(\mathbf{r}) = \exp(\mathbf{ik} \cdot \mathbf{r})\mathbf{u_k}(\mathbf{r}), \tag{2.70}$$

where $u_k(\mathbf{r})$ is periodic in space with the same periodicity with the cell which can be expanded into a set of plane waves

$$u_i(\mathbf{r}) = \sum_{\mathbf{G}} c_{i,\mathbf{G}} exp(i\mathbf{G} \cdot \mathbf{r}) \tag{2.71}$$

Combining eq. (2.70) and (2.71, each electronic wave function can be expressed as

$$\Psi_i(\mathbf{r}) = \sum_{\mathbf{G}} c_{i,\mathbf{k+G}} exp(i(\mathbf{k} + \mathbf{G}) \cdot \mathbf{r}) \tag{2.72}$$

Kohn-Sham equation in eq. (2.49) is substitute in terms of reciprocal space **k** as below:

$$\sum_{\mathbf{G'}} \left[\frac{1}{2} |\mathbf{k+G}|^2 \delta_{G,G'} + V_{KS}(\mathbf{G\text{-}G'}) \right] c_{i,\mathbf{k+G}} = \varepsilon_i c_{i,\mathbf{k+G}} \tag{2.73}$$

Solution of the Kohn-Sham equation can be obtained by diagonalization of the Hamiltonian matrix. The diagonal part is the kinetic term, otherwise are the potential term. To limit the summation over **G**, cut off energy is applied to the kinetic term which is expressed by

$$E_{cut} = \frac{1}{2} |\mathbf{k+G}|^2 \equiv \mathbf{G}_{cut}^2 \tag{2.74}$$

The limitation of the energy is reasonable due to the fact that lower energy is more important.

2.5 Pseudopotential

The maximum number of plane waves is required to expand the tightly bonded core electrons due to rapid oscillation near the nuclei. However, valence electrons greatly affect far more than the core electrons of the electron structure of the material. The concept of a pseudopotential is the replacement of one problem with another. The primary application in electronic structure is to replace the strong Coulomb potential of the nucleus and the effects of the tightly bound core electrons by an effective ionic potential acting on the valence electrons. A pseudopotential can be generated in an atomic calculation and then used to compute properties of valence electrons in molecules or solids, since the core states remain almost unchanged. Furthermore, the fact that pseudopotential are not unique allows the freedom to choose from that simplify the calculations and the interpretation of the resulting electron structure. There are two types of famous pseudopotential, norm conserving pseudopotential and ultrasoft pseudopotential

2.5.1 Norm Conserving Pseudopotential

In this kind of pseudopotential, there are some requirements to be fulfilled [13]. Those requirements are

1. All the electrons and pseudo valence eigenvalues are the same as the selected atomic configuration.

$$\epsilon_i^{AE} = \epsilon_i^{PS} \tag{2.75}$$

2. All the electrons and pseudo valence eigenvalues are in agreement in an external core region.

$$\Psi_i^{AE}(r) = \Psi_i^{PS}(r), \quad r \geq R_c \tag{2.76}$$

3. The logarithmic derivatives and their first energy derivative of real and pseudo wavefunctions match at the cut-off radius R_c.

$$\frac{d}{dr} \ln \Psi_i^{AE}(r) = \frac{d}{dr} \ln \Psi_i^{PS}(r) \tag{2.77}$$

4. The total charge inside core radius R_c for each wave function must be same (norm conservation).

$$\int_0^{R_c} dr |\Psi_i^{AE}(r)|^2 = \int_0^{R_c} dr |\Psi_i^{PS}(r)|^2 \tag{2.78}$$

5. The first energy derivative of the logarithmic derivatives of all-electron and pseudo wave functions must be same for $r \geq R_c$. This condition is implied by point 4.

2.5.2 Ultrasoft Pseudopotential

This pseudopotential releases norm conservation criteria to obtain smoother pseudo wave functions [14]. The pseudo wave functions are divided into two parts:

1. Ultrasoft valence wave functions which omit norm conservation criteria ϕ_i^{US}.

2. A core augmentation charge.

$$Q_{nm}(r) = \Psi_n^{AE*}(r)\Psi_m^{AE}(r) - \Psi_n^{US*}(r)\Psi_m^{US}(r) \tag{2.79}$$

The ultrasoft pseudopotential takes the form of

$$V^{US} = V_{loc}(r) - \sum_{nmI} D_{nm}^0 |\beta_n^I\rangle\langle\beta_m^I| \tag{2.80}$$

where β is projector function which is expressed by

$$|\beta_n\rangle = \sum_m \frac{|X_m\rangle}{\langle X_m|\phi_n\rangle} \tag{2.81}$$

and they are strictly localized inside the cut-off region for the wave functions since the X - functions are defined through

$$|X_n\rangle = (\epsilon_n - \hat{T} - V_{loc})|\phi_n\rangle \tag{2.82}$$

$$D_{nm}^0 = \langle\phi_n\rangle|X_m\rangle + \epsilon_m q_{nm} \tag{2.83}$$

The scattering properties of the pseudopotential can be improved by using more than one β projector function per angular momentum channel.

It is necessary to use generalized eigen value formalism. For this case we introduce the overlap operator S

$$\hat{S} = \mathbf{1} + \sum_{nmI} q_{nm}|\beta_n^I\rangle\langle\beta_m^I| \tag{2.84}$$

where

$$q_{nm} = \int_0^{r_c} dr Q_{nm}(r) \tag{2.85}$$

Then the charge density is expressed by

$$\begin{aligned} n(\mathbf{r}) &= \sum_i \phi_i^*(r)\hat{S}\phi_i(r) \qquad (2.86)\\ &= \sum_i \left[|\phi_i(\mathbf{r})|^2 + \sum_{nmI} Q_{nm}^I(\mathbf{r})\langle\phi_i|\beta_n^I\rangle\langle\beta_m^I|\phi_i\rangle \right], \end{aligned}$$

2.6 Formation Energy and Energy Barrier

In Chapter 3, as the studied system having same element, we will refer formation energy E_f which is defined as

$$E_f = E_d - \frac{N_d}{N_p} E_p, \tag{2.87}$$

where E_{dt} and E_p are the total energies of the defect system and the perfect system, respectively; N_d and N_p are the numbers of the atoms in the defect system and the perfect system, respectively.

In the healing energy calculation of adatom-vacancy pair in graphene, we use the constrained optimization method.[33] First, between the initial and final geometries, we sample the hyper-planes(Fig.2.1.a). Then, we calculate the atomic force component which is parallel to each hyper-plane, and optimize the geometry on the hyper-plane for each sample(Fig.2.1.b). Among these optimized geometries, the geometry having the highest total energy corresponds to the transition state. And the energy difference between the initial E_{tr} and the transition state E_{tr}, is the energy barrier E_b (Fig.2.2) which is

$$E_b = E_{tr} - E_i. \tag{2.88}$$

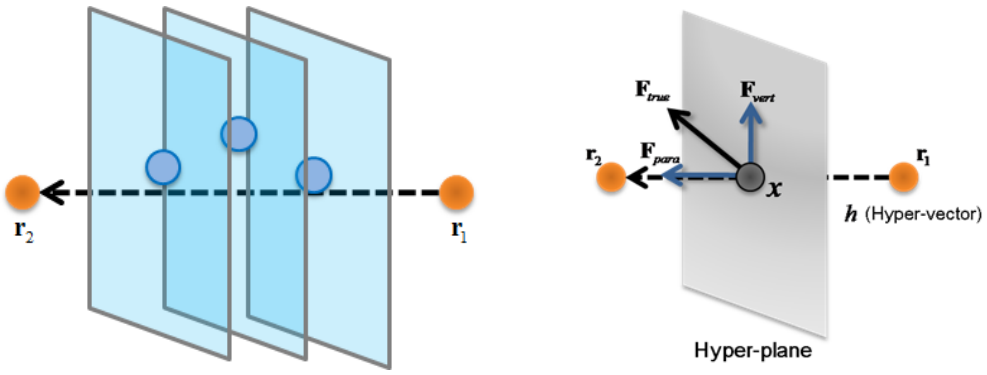

(a) Hyper planes from initial to final

(b) Geometry optimizing on the hyper plane

Figure 2.1: The constrained optimization method for energy barrier

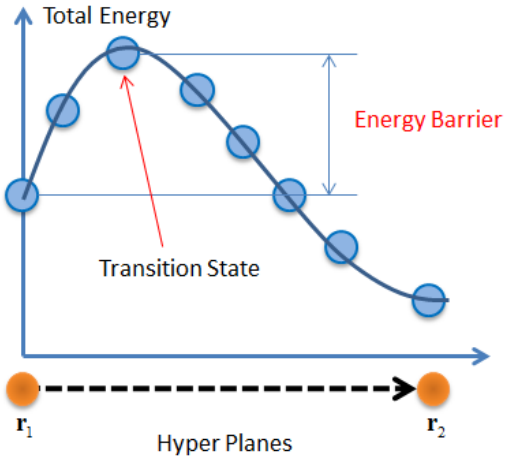

Figure 2.2: The energy barrier

2.7 Electron-Positron Density Functional Theory (EPDFT)

In the positron annihilation study, the electron-positron density functional theory (e-p DFT) is obbligato.[44, 45, 47] We first perform standard electron band structure calculations based on the spin-polarized GGA. Then, we calculate the positron wave function by using the following equation based on the local density approximation for the electron-positron correlation,[45]

$$\{-\frac{1}{2}\nabla^2 - \int dr' \frac{n_e(r') - n_0(r')}{|r - r'|} + \mu_{e-p}(n_e)\}\psi_i^+(r) = \varepsilon_i^+\psi_i^+(r) \tag{2.89}$$

where n_e, n_p, and n_0 are the electron, positron and nuclear charge densities, respectively, and $\mu_{e-p}(n_e)$ is the potential due to electron-positron correlation. After we obtain the electron ($n_e^{\uparrow(\downarrow)}$) and positron ($n_p$) densities, the positron lifetime $\tau^{\uparrow}(\tau^{\downarrow})$ for the majority (minority) spin can be calculated as

$$\frac{1}{\tau^{\uparrow(\downarrow)}} = \pi r_e^2 c \int dr n_e^{\uparrow(\downarrow)}(r) n_p(r) \Gamma(n_e) \tag{2.90}$$

where r_e is the classical electron radius and c is the light velocity. $\Gamma(n_e)$ is the enhancement factor.

In the above computational scheme, we assume that the correlation potential $\mu_{e-p}(n_e)$ does not depend on the electron spin-polarization. The calculation of the correlation energy for a single positron in the homogeneous non-polarized electron gas was performed based on the random phase approximation by Arponen and Pajanne [48] and the numerical results were fitted

to an analytic function by Puska, Seitsonen, and Nieminen (PSN)[45]. The enhancement factor $\Gamma(n_e)$ is also deduced from numerical results for a single positron in the homogeneous non-polarized electron gas. The calculation was performed by Lantto [46], who used hyper-netted chain method and the numerical results are fitted to an analytical function by PSN[45].

$$\Gamma(n_e) = 1 + 1.23r_s + 0.9889r_s^{3/2} - 1.4820r_s^2 + 0.3956r_s^{5/2} + r_s^3/6, \tag{2.91}$$

where $(4\pi/3)r_s^3 = 1/n_e$.

The above scheme based on the electron-positron DFT has been applied to various materials and was found to give reliable results for non-spin-polarized systems[47, 49, 50, 51]. However, applications to spin-polarized materials are very rare. The purpose of the positron lifetime calculations in the later chapter is to clarify the validity of the above mentioned scheme for ferromagnetic materials.

2.8 Calculation Details

In chapter **3**, we use the spin-polarized generalized gradient approximation (GGA) within the density functional theory (DFT). Ultrasoft pseudopotential and plane wave basis set whose maximum kinetic energy is 25 Ry are used. In the optimized geometry of the graphite, the bond length is 1.42 Å, which is the same as the experimental value (1.42 Å). We use the 128-site supercell with the rectangle shape of the 17.04 $\times$ 19.68 Å^2 size. This size corresponds to the lattice constant of the pristine graphite. The sampling point in the two-dimensional Brillouin zone integration is 4.

We calculate the formation energy which is measured from the energy of the pristine structure, i.e., the formation energy is defined as the difference between the total energy of the defect system in the supercell and the multiplication of the energy of the perfect structure sheet per atom and the number of the atoms in the supercell.

In determining the diffusion barrier, we use the constrained optimization method as mentioned in this chapter 2.2.

In chapter 4, we use the spin-polarized generalized gradient approximation (GGA) within the electron-positron density functional theory (e-p DFT). In numerical calculations, we adopt ultrasoft pseudopotentials and plane waves. The method of application of ultrasoft pseudopotentials and plane waves to the calculations of positron lifetimes was presented in a previous paper.[47]

The ferromagnetic metals, Fe, Co, and Ni form bcc, hcp, and fcc structures in room temperature, respectively. We use the experimental lattice constants for Fe (2.8675 $\mathring{A}$)[53], Co (2.5074 $\mathring{A}$ and 4.0699 $\mathring{A}$ for the a and c lattice constants), and Ni (3.524 $\mathring{A}$)[54], respectively. The k-points used in calculations are 60x60x60, 30x30x18, and 50x50x50, for Fe, Co, and Ni, respectively. The cut off energy of wavefunction is 340 eV for electrons and 680 eV for a positron, and the cut off energy of charge density is 3040 eV.

Chapter 3

Healing of Adatom-vacancy Pair Defects in Graphene

In Chapter 1, we mentioned our study related to the healing of adatom-vacancy pair defect in carbon nano-materials. And in Chapter 2, the theory and methods are introduced to solve the problem of healing of defects. Here, we will demonstrate the detail of this study.

3.1 Introduction

Nowadays, the semiconductor device is commonly used in electronic products. The semiconductors are developing because of down sizing to several nano-meters, and we need to control devices on the atomic level. Then, the control of defects and impurities is necessary. The experimental methods are considered to be not so sufficient to observe the atomic level phenomenons. However, the computational methods are expected to study these problems much efficiently.

Carbon nano-materials such as graphenes and nanotubes have attracted much attention since they are candidates for post-silicon device materials. Compared with conventional silicon devices, the effects of defects on carbon nano-device are expected to be serious because of the low dimensional conductivity. Therefore, the study of defects in sp^2 carbon systems is undertaken.

Thus far, pentagon-hexagon pairs [15], mono- and multi-vacancies [16, 17, 18, 19, 20, 21, 22], adatoms [23, 24], adatom dimers [25], and adatom-vacancy pairs [26] have been studied.

Among various defects, adatom related defects were observed at low temperatures. Recently low-energy electron irradiation on single-walled carbon nanotubes (SWCNTs) was performed[28]. The observation of I-V characteristic shows that some defects having some band gaps are created at low temperature by irradiation. Scanning tunneling microscope (STM) with the bias of 4.5 V at low temperature (95 K) also induces some unknown defects having band gaps[29, 30]. These defects are expected to be related to adatoms which can be created by electron irradiation or STM. Then, a hydrogen thermal desorption spectroscopy treat the defects induced by low-energy electron irradiation in SWCNTs. And it shows that some defects are healed at 44-70 K[31]. It is expected that the observed defect was the adatom-vacancy pair. However, it is still no theoretical study to confirm this completely. Thus, it is emerge to have a theoretical study to understand this kind of defect better.

Graphene, as a SWCNT with infinite radius, is a good sample for investigating the defects. A previous calculation of graphene found that the energy barrier is 0.47 eV for migration of one adatom[32]. A past study based on first-principles calculation clarified the energy barrier (0.49 eV) of migration of one adatom[33].

The purpose of this chapter is to make sure if the defect induced by low-energy electron irradiation is the adatom-vacancy pair by performing the numerical healing barrier calculations, and also to make sure if the adatom tends to return to the vacant site or to immigrate to other position. The results of the energetic stable structures and the healing barrier of adatom-vacancy pairs will be described. We first investigate the healing of the adatom bonded to a nearest atom of the vacancy site. Then we investigate the case of the adatom bonded to an atom which is 4.26-5.54 Å far from the vacancy site.

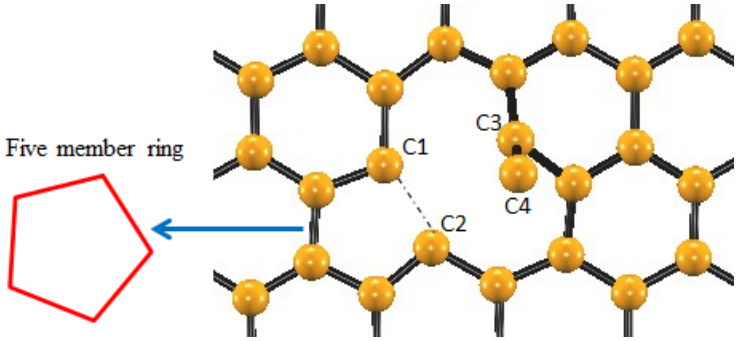

Figure 3.1: Adatom-vacancy pair when the adatom is bonded to a nearest site of the vacancy in the graphene.

3.2 The Adatom Bonded to A Nearest Atom of The Vacancy Site

We perform calculations on the adatom-vacancy pair in graphenes (Fig. 3.1). We find that there is stable geometry when the adatom is bonded to a nearest atom of the vacancy. The calculated formation energy is 9.83 eV. Due to the relaxation, the distance between the two nearest atoms (C1 and C2 in Fig. 3.1) becomes small, and then the five-member ring is formed (Fig. 3.1). The bond length between the two nearest atoms (C1 and C2) is found to be 1.85 Å, which is longer than that of graphene (1.42 Å). So the interaction between the two atoms is weak compared with that of the graphene bond. Then, we investigate the healing barrier of this adatom-vacancy pair. The position of the adatom in the transition state is slightly (0.05 Å) far from that in the stable structure of the adatom-vacancy pair. Since the transition state geometry is close to that of the stable adatom-vacancy pair, the healing barrier energy is very small (0.06 eV). Therefore, this adatom-vacancy pair defect can be healed at very low temperature. The barrier is much lower than that of the adatom diffusion barrier which was estimated to be 0.49 eV in our previous calculation[33].

Here, we compare our results with previously reported ones for different systems. The recombination process of the interstitial and vacancy pair in the graphite[27] is similar to the healing one in the present system. However, the previously calculated energy barrier of the

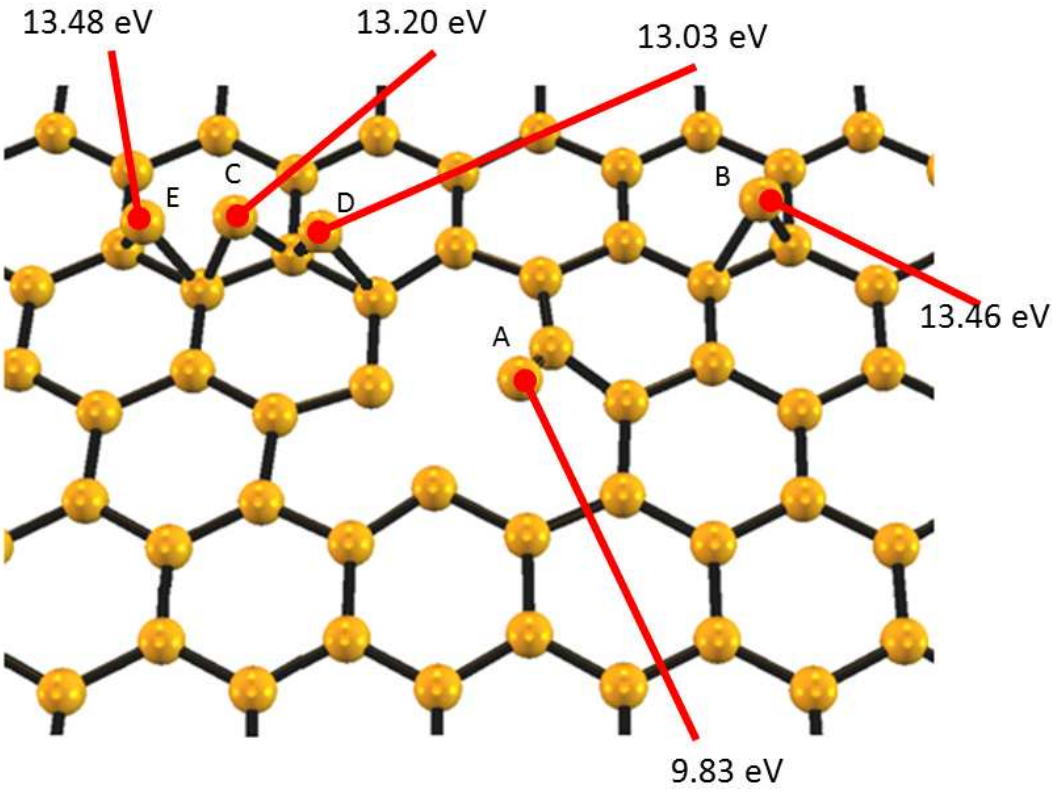

Figure 3.2: Formation energies of the adatom-vacancy pairs in the graphene.

recombination (1.3 eV)[27] was much higher than that the healing barrier (0.06 eV) of the present system. This large barrier for the recombination is due to the fact that the interstitial atom in the stable geometry of the interstitial and vacancy pair is bonded to a nearest carbon atom of the vacancy and also the two carbon atoms which are located on the nearest graphite layer. In this recombination process, large energy is necessary to break these three bonds. On the other hand, in our present system, the adatom in the stable state is bonded to only a nearest carbon atom of the vacancy since the system consists of a single graphene layer. Therefore, the very low healing barrier of the present is expected to be intrinsic for the mono-layer graphene.

3.3 The Adatom Bonded to An Atom Which is 4.26-5.54 Å Far From The Vacancy Site

We investigate the cases that the adatom is located a little bit far from the vacancy site. We try several sites which are 4.26-5.54 Å far from the vacant site as shown in Fig. 3.2 and confirm the energetical stability of the geometries. We find that the formation energies are 13.46, 13.20, 13.03, and 13.48 eV, for the B, C, D, and E geometries, respectively. These values are larger than the value of geometry A where the adatom is bonded to a nearest atom of the vacancy (9.83 eV), which has been studied in the previous section. We expect that when the energy injected into the pristine graphene is somewhat larger than that induces the adatom-vacancy pair of geometry A, the defects of B-E are created. This energy injection is expected to be achieved by STM and electron irradiation experiments[28, 29, 30].

Then, we calculate the healing barriers of C and D since their total energies are relatively small. First, we calculate the healing barriers of geometry C (Fig. 3.3(a)) and geometry D (Fig. 3.3(b)). We find that there are two transition states between geometry C and the perfect geometry as Fig. 3.3 shows. The first transition state (Fig. 3.3(c)) is located between geometry C and geometry D, where the energy of D is 0.17 eV lower than that of C. The total energy of this transition state is 0.24 eV higher than that of geometry C. The second transition state (Fig. 3.3(d)) is located between geometry D (Fig. 3.3(b)) and the perfect geometry. The total energy of this transition state is 0.23 eV higher than that of geometry D. Therefore, we conclude that the healing barrier of geometry C is 0.24 eV and that of geometry D is 0.23 eV.

We next carry out calculations on the healing barrier of geometry B (Fig. 3.4(a)). It is find that the transition state (Fig. 3.4(b)) is located between geometry B and geometry A (Fig. 3.2). The totoal energy difference between this transition state and geometry B is 0.32 eV. As the healing barrier of geometry A is very smaller (0.06 eV), we therefore conclude that the healing barrier of geometry B is 0.32 eV.

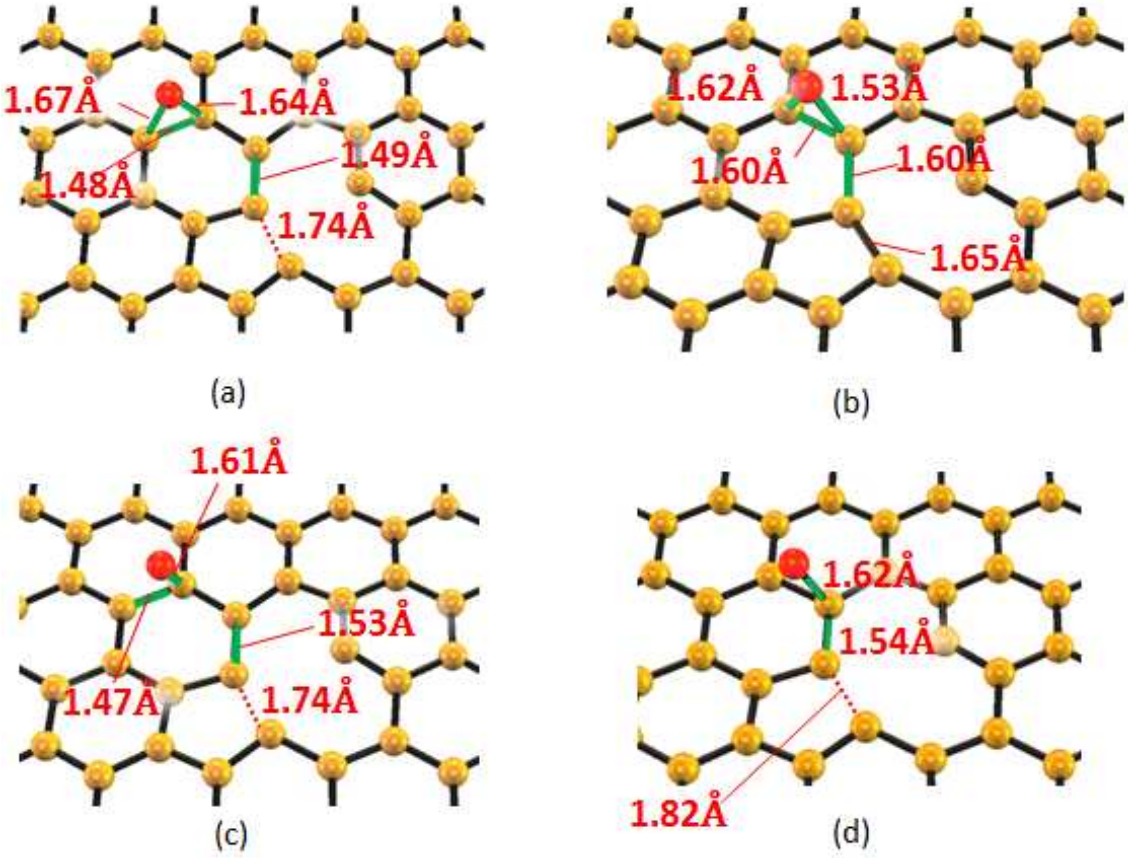

Figure 3.3: Healing path of geometry C and D. Geometry C and geometry D are shown in (a) and (c), respectively. Two transition states are shown in (b) and (d).

3.4 Analysis of Spin Density of Adatom-Vacancy Pair Defects

We investigate the magnetic property of the adatom-vacancy pair defects in graphene. We find that among the geometries studied (Fig.3.2), the geometries B and C have magnetic property. The electron spin differences are shown in Fig.3.5. The atom C1 and C3 which lost a bond comparing with the other two atoms belong to the just formed five-member ring, have the similar spin shape considered to be a sp-orbital. In the geometry B (Fig.3.5.(a)), the adatom C2 has no spin, while in the geometry C (Fig.3.5.(b), the adatom C4 has spin considered to be a p-orbital.

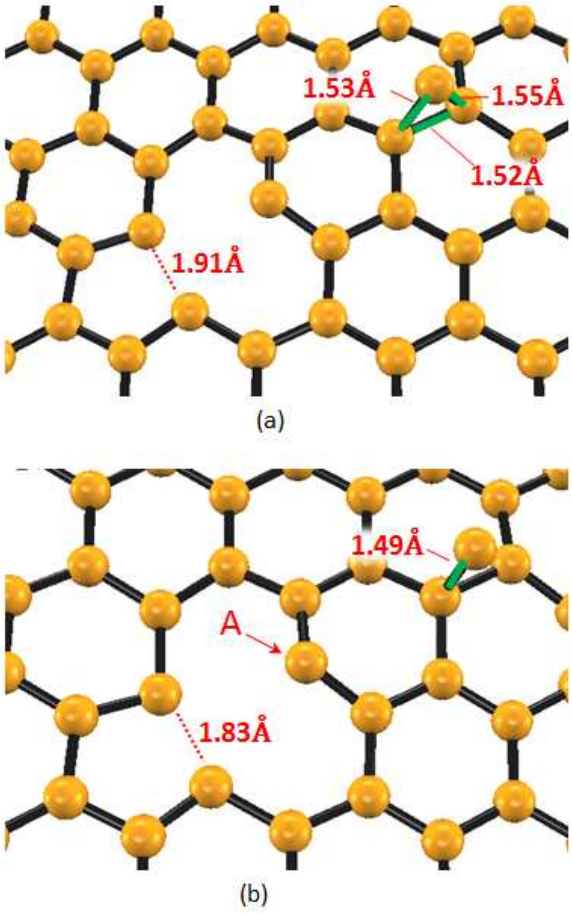

Figure 3.4: Adatom-vacancy pair when the atom little (5.54 Å) far from the vacancy in graphene (a) and the transition geometry (b).

3.5 Discussion

In this study we have investigated the adatom-vacancy pair in graphenes by carrying out first-principle calculations based on the spin-polarized GGA. We found that when the adatom is bonded to the nearest adatom of vacancy (geometry A), the healing barrier is very small (0.06 eV) and therefore this defect can be easily healed in low temperature which is consistent with the experiment of the hydrogen thermal desorption spectroscopy in the temperature 44-95 K[31].

We have also performed calculations for the case that the adatom is located 4.26-5.54 Å far from the vacant site. The formation energies were found to be larger than that of geometry A.

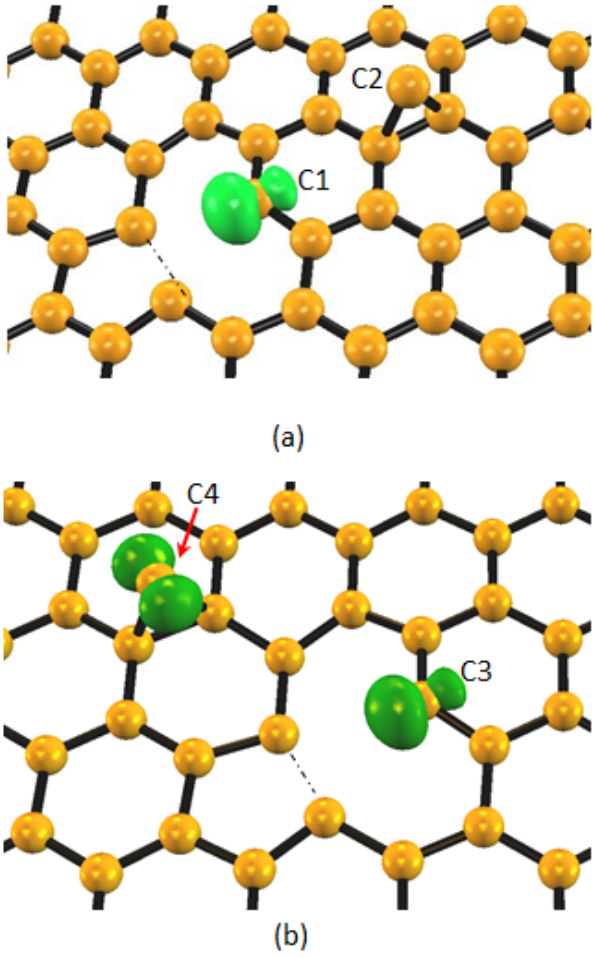

Figure 3.5: Magnetic property of adatom-vacancy pair.

Therefore, we expect that these defects are created when the energy injected into the pristine graphene is somewhat larger than that induces the adatom-vacancy pair of geometry A. We find that the healing barriers are 0.24-0.32 eV. These values are larger than that of the geometry A but are smaller than that of the adatom diffusion barrier (0.47-0.49 eV) [32, 33]. Therefore the defects having geometries B, C, and D are expected to be healed in the low temperature range where the adatom does not diffuse. We also find that geometries B and C have magnetic property.

Here, we discuss the case when the adatom is bonded to the nearest atom of the vacancy site comparing with the adatom-vacancy pair defect in some kinds of SWCNTs. Other group [26] reported that in several SWCNTs ((9,0), (10,0), and (11,0)), It is found that the bond lengths

in the five-member ring (corresponding to C1-C2 in Fig. 3.1) are 1.50, 1.52, and 1.54 Å for the (9,0), (10,0), and (11,0) SWCNTs, respectively. These lengths are much smaller than the present length of C1-C2 bond (1.85 Å) of the graphene. Since these somewhat strong bonds in SWCNTs need large energy to break , the healing barriers are expected to be large. Indeed, the healing energies of adatom-vacancy pair in SWCNTs are estimated to be 1.26-2.24 eV which is larger than the present value for the graphene (0.06 eV). The radii of these SWCNTs are $\sim$0.8 nm. Since the graphene corresponds to the SWCNT having the infinite radius, we therefore expect that the healing barrier becomes low when the radii of the CNT increases.

Chapter 4

Positron annihilation studies on ferromagnetic metals

In Chapter 1, we mentioned our study related to spintronics with spin-polarized positron annihilation method. And in Chapter 2, the method of electron-positron DFT (EPDFT) is described for the calculation of positron annihilation. We would like to show the detail of this study in this chapter.

4.1 Introduction

Recently, spin-polarized positron experiment attracts scientific attention because of application to the study of electron spin phenomena.[34, 35] Low-energy spin-polarized positron beams enable us to study magnetism at surfaces, interfaces and in thin films. Positrons are trapped by vacancy defects, so spin-polarized positron annihilation spectroscopy (SP-PAS) is expected to be an useful tool to study vacancy induced magnetism [36]. Ferromagnet is one of fundamental spin polarization materials. Therefore, to detect spin-polarization in ferromagnet by using SP-PAS is scientifically important.

The 3γ spin-polarized positron experiment on ferromagnetic materials was first carried out by Berko in 1971[37]. Later, two-dimensional two-photon angular correlation of the spin-

Table 4.1: Non-spin-polarized positron lifetimes (ps) for the bulk Fe, Ni, and Co.

elements	theory	experiment
Fe	101.79	106^a
Co	96.25	110^b
Ni	99.04	118^a

a: Ref[42] b: Ref[43]

polarized positron annihilation radiation in Ni[38, 39, 40] and Co[41], and the Doppler broadening of annihilation radiation[34, 35] were measured. These experiments allow us to get information on the spin polarization in ferromagnetic materials. Then, it is expected that positron annihilation experiment can be applied to study spintronics. There are still few theoretical studies on spin-polarized positron.

In this study, we choose the ferromagnetic metals Fe, Co, Ni, and Gd as the samples for the reason that thet are common materials can be possible applied to experiment for comparing. So, we perform the calculations on the lifetimes of spin-polarized positrons in Fe, Co, Ni, and Gd by using EPDFT. We investigate both the non-spin-polarized case and the spin-polarized case. The lifetime difference ($\tau^{\downarrow}$-$\tau^{\uparrow}$) is expected to be positive, but it is found to be negative in the case of Ni. This negative value of Ni is consistent with the $P^{3\gamma}$ experiment done by Berko[37]. We will explain the origin of it in this chapter.

4.2 Non-spin-polarized case

First, we calculate the lifetimes of non-spin-polarized states of Fe, Co, and Ni (Table 4.1). These calculations well reproduce the experimental results, though the calculated values are slightly smaller than the experimental values.

Table 4.2: Spin-polarized positron lifetimes for the bulk Fe (bcc), Co (hcp), Ni (fcc), and Gd (hcp). We also show the spin moments ($\mu B/atom$).

elements	spin moment(μB/atom)			lifetime(ps)		
	majority spin	minority spin	total magnetic moment	$\tau^{\uparrow}$	$\tau^{\downarrow}$	$\tau^{\downarrow}-\tau^{\uparrow}$
Gd	12.837	-5.164	7.673	175.694	255.049	79.355
Fe	5.156	-2.844	2.311	95.159	107.008	11.849
Co	5.319	-3.681	1.637	94.493	98.245	3.752
Ni	5.473	-4.527	0.945	101.129	96.764	-4.365

4.3 Spin-polarized case

Next we study the spin-polarized states of Fe, Co, Ni, and Gd (Table 4.2). We find that the lifetime differences between majority spin electrons and minority spin electrons($\tau^{\downarrow}-\tau^{\uparrow}$) are 11.85 ps, 3.75 ps, -4.37 ps and 79.34 ps for Fe, Co, Ni, and Gd, respectively.

Surprisingly, we find that the value for Ni (-4.365 ps) is negative since the annihilation rate is expected to be large when the electron number is large. However, the negative sign of the lifetime difference in Ni is consistent with the 1970s three photon polarization measurement experiment result[37] as is discussed here. First, the experimentally observed $P^{3\gamma}$ is given by the following equation:

$$P^{3\gamma}=\frac{N_{+}^{3\gamma}-N_{-}^{3\gamma}}{N_{+}^{3\gamma}+N_{-}^{3\gamma}} \tag{4.1}$$

where $N^{3\gamma}=\int dpN^{3\gamma}(p)$, $N^{3\gamma}(p)$ is the electron momentum distribution from three photon positron annihilation experiment. By using the experimental values of $N_{\pm}^{3\gamma}$, we evaluate $P^{3\gamma}$, which is denoted by $P_{expt}^{3\gamma}$ in Table 4.3. The $P^{3\gamma}$ is also given by,

$$P^{3\gamma}=-\frac{(\tau^{\downarrow}-\tau^{\uparrow})(\tau^{\downarrow}+\tau^{\uparrow})}{\tau^{\downarrow 2}+\tau^{\downarrow}\tau^{\uparrow}+\tau^{\uparrow 2}}P^{p} \tag{4.2}$$

where $\tau^{\uparrow}$ and $\tau^{\downarrow}$ are the positron lifetimes for majority and minority spins, respectively, and P^{p} is the positron polarization. We evaluate $P^{3\gamma}$ in Eq.(5) by using the calculated positron lifetimes ($\tau^{\uparrow}$ and $\tau^{\downarrow}$) and the experimental value of P^{p} (0.35).[56] This evaluated value is denoted by $P_{theory}^{3\gamma}$ in Table 4.3. Our calculated values ($P_{theory}^{3\gamma}$) are comparable with the experimental

Table 4.3: $P^{3\gamma}$ from three photon polarization measurement

elements	P_{theory}	$P^{3\gamma}_{expt}$ [a]
Fe	-0.0273	-0.0053±0.0009
Co	-0.0091	-
Ni	+0.0103	+0.0012±0.0009
Gd	-0.0850	-0.0091±0.0018

a: Ref[37]

values ($P^{3\gamma}_{expt}$); though the theoretical absolute value of Fe is 5.1 times larger than the experimental value. The difference may be due to some inaccuracy of the experiment. It should be emphasized that the signs of the theoretical values of $P^{3\gamma}$ are the same as those of the experimental ones. The positive value of Ni indicates the negative positron lifetime difference ($\tau^{\downarrow}$-$\tau^{\uparrow}$).

4.4 Explanations for the negative lifetime difference ($\tau^{\downarrow}$-$\tau^{\uparrow}$) in Ni

Then, we analyse the electronic structures to find the reasons for the negative lifetime difference in Ni. We check the projected density of states (PDOSs) for the atomic orbitals of $3d$ and $4s$ with radius 1.5 $bhor$ (Fig.4.1).

In the cases of Fe, Co, and Ni, the $4s$ components are very small compared with $3d$ components. It is also found that the distributions of PDOSs of d orbitals in the three materials are similar to the total DOSs (see Figs.4.2 (a) - (c)), indicating that the d orbital components are very larger than those of the s orbitals. Therefore, the $3d$ electrons are considered to dominate the positron lifetime.

It is obviously found that the magnetic moment decreases as the atomic number increases: the calculated magnetic moments per atom are 2.311μB, 1.637μB, 0.945μB, and 7.673μB for Fe, Co, Ni, and Gd respectively (see Table 4.2). As the magnetic moment decreases, the differ-

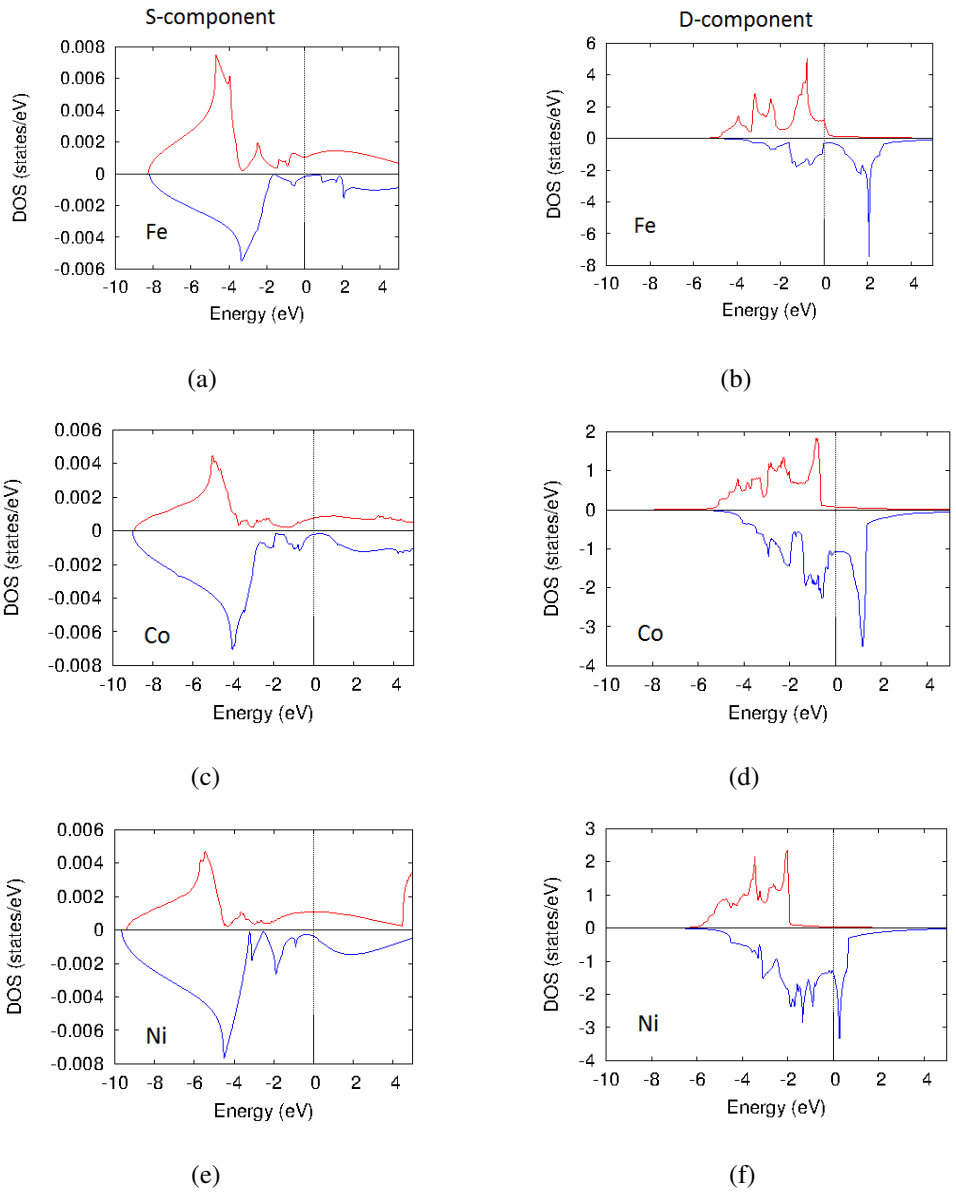

Figure 4.1: Atomic projected density of states.

ence between the numbers of the majority spin and minority spin electrons becomes small, then the lifetime difference ($\tau^{\downarrow}$-$\tau^{\uparrow}$) is expected to be small. This expectation is consistent with our calculational results that the positron lifetime difference becomes small as the atomic number increases (Table 4.2).

However, the origin of the negative lifetime difference for the Ni case is still unresolved. Here, we analyse the electron and positron distributions of Fe and Ni and discuss the negative

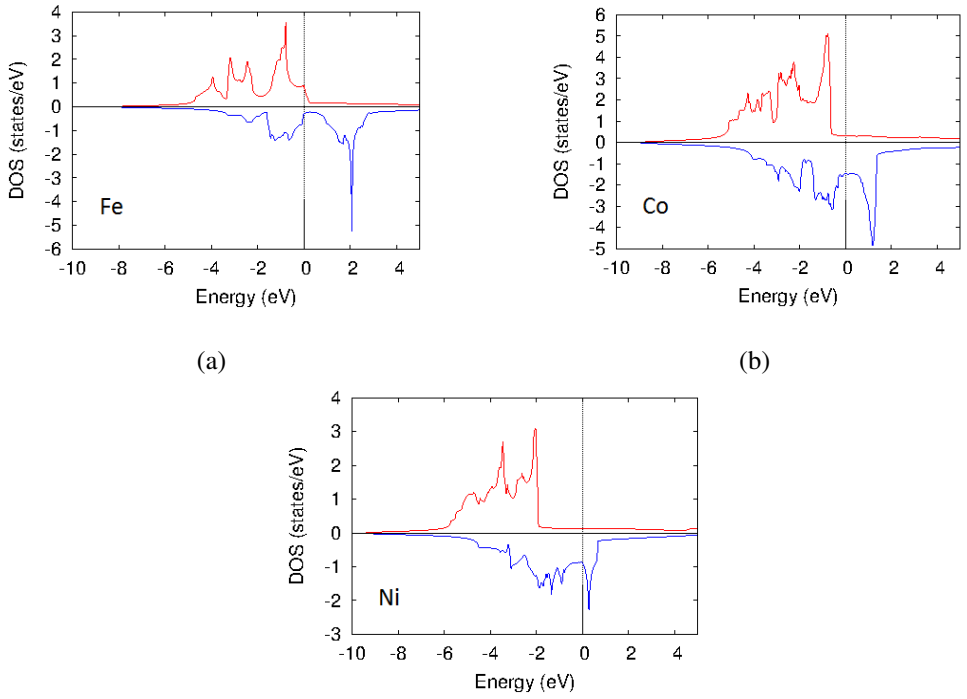

Figure 4.2: Spin density of states:(a)Fe, (b)Co, and (c)Ni.

value of Ni. In the case of Ni, the charge density of the minority spin is delocalized and thus the densities in the interstitial regions are larger than those of the majority spin [Figs4.3.(a) and (b)] We find that the charge density of the positron is localized in the interstitial regions (Figure.4.3.(d)). Since the density of the minority spin is large in the interstitial region, the overlaps S_{e-p} are larger than those for the majority spin (Figs.4.3.(f) and (g)), where S_{e-p} is defined as

$$S_{e-p} = n_e^{\uparrow(\downarrow)}(r) n_p(r) \Gamma(n_e) \tag{4.3}$$

This large electron-positron overlap for the minority spin is the reason for the negative lifetime difference.

Next, in the case of Fe, we also find that the minority spin electrons have broad distribution and thus the charge densities in the interstitial regions are larger than those for the majority spin (Figs.4.4.(a) and (b)). The positron charge density has the maximum in the interstitial region as similar as in the case of Ni (Figure.4.4.(d). However, the electron-positron overlap distribution is quite different from that of Ni: since the electron spin polarization is large in the case of Fe,

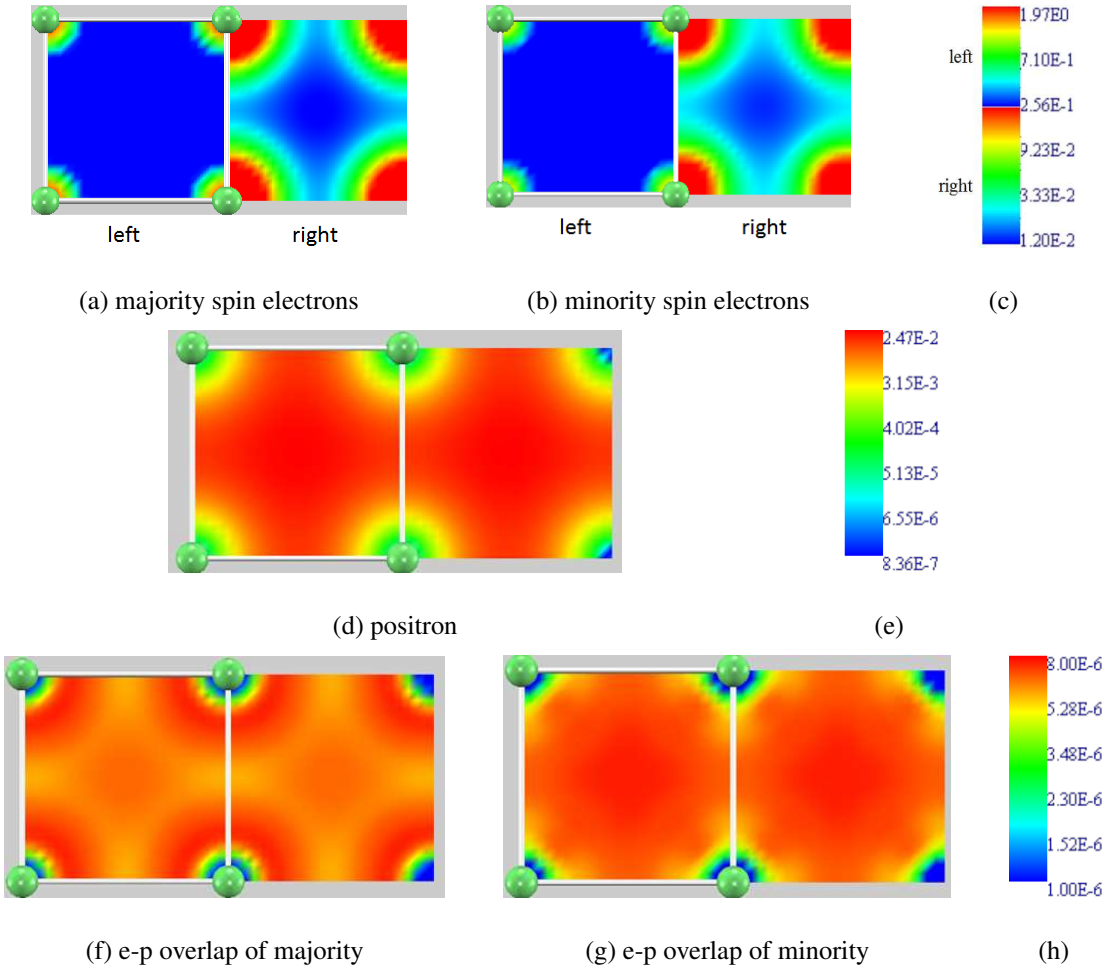

(a) majority spin electrons (b) minority spin electrons (c)

(d) positron (e)

(f) e-p overlap of majority (g) e-p overlap of minority (h)

Figure 4.3: Spin densities of electron ((a) and (b) with the different color bars as left and right), density of the positron (d), and electron-positron overlaps ((f) and (g)) in the case of Ni of the [110] direction. The units in (a), (b), and (d) are $e/(au)^3$, and those in (f) and (g) are $e^2/(au)^6$, respectively.

the electron-positron overlap for the majority spin is generally larger than that for the minority spin (Figs.4.4). This result leads to the fact that the lifetime difference is positive in the case of Fe.

It is also necessary to check the cases of Co and Gd. We again find that the charge density of the minority spin in the case of Co is rather broad compared with that of the majority spin, and the positron is localized in the interstitial region.(Fig.4.5) Since the magnetic moment of Co is large, the lifetime difference is positive as in the case of Fe.

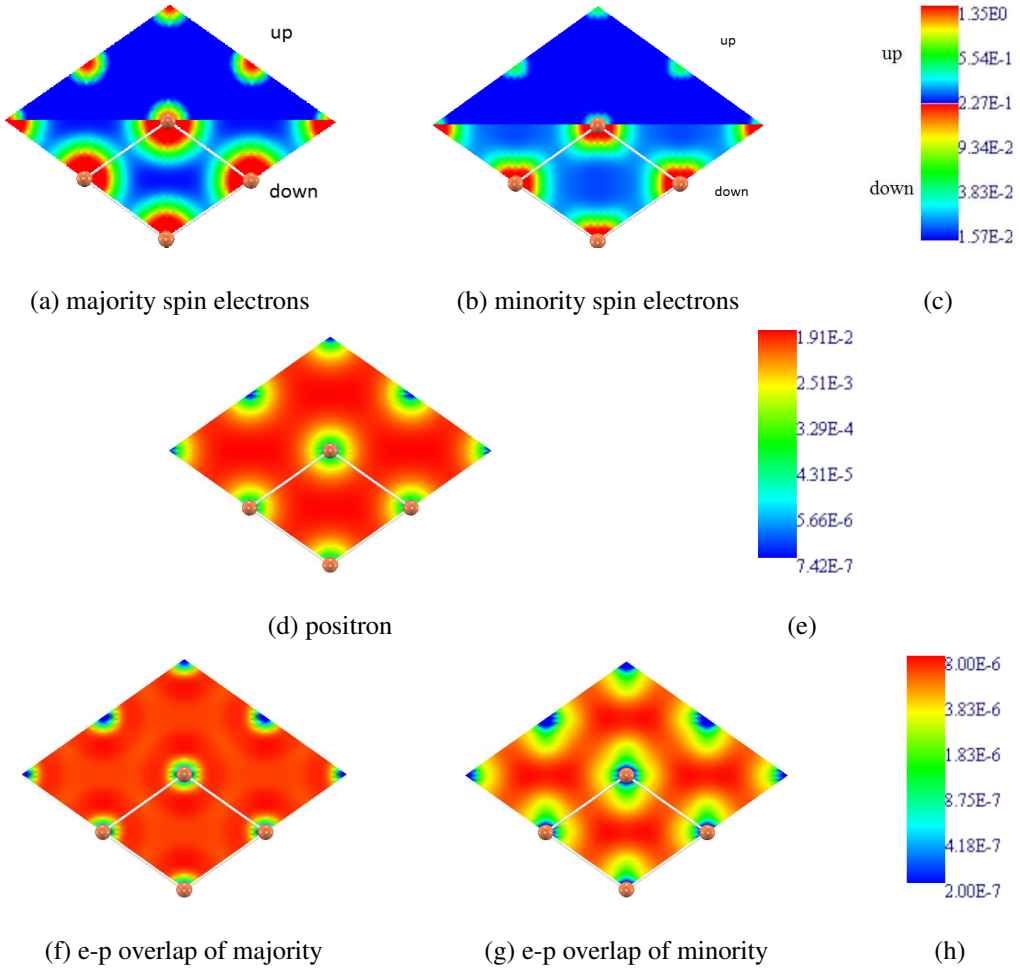

(a) majority spin electrons (b) minority spin electrons (c)

(d) positron (e)

(f) e-p overlap of majority (g) e-p overlap of minority (h)

Figure 4.4: Spin densities of electron ((a) and (b) with different color bar as up and down), density of the positron (d), and electron-positron overlaps ((f) and (g)) in the case of Fe of the [110] direction. The units in (a), (b), and (d) are $e/(au)^3$, and those in (f) and (g) are $e^2/(au)^6$, respectively.

The magnetic moment is very large ($7.673\mu B$) in the case of Gd, and the delocalized distribution of the minority electrons also appears (Fig.4.6.(f) and (g)).

So far, we found that the distribution of the minority spin is broad for Fe, Co, Ni and Gd. We also found that the positron distributions have the maxima in the interstitial regions. As a result, the lifetimes difference in Ni is negative. However, in the cases of Fe, Co, and Gd, the lifetimes differences are positive since the magnetic moments are large.

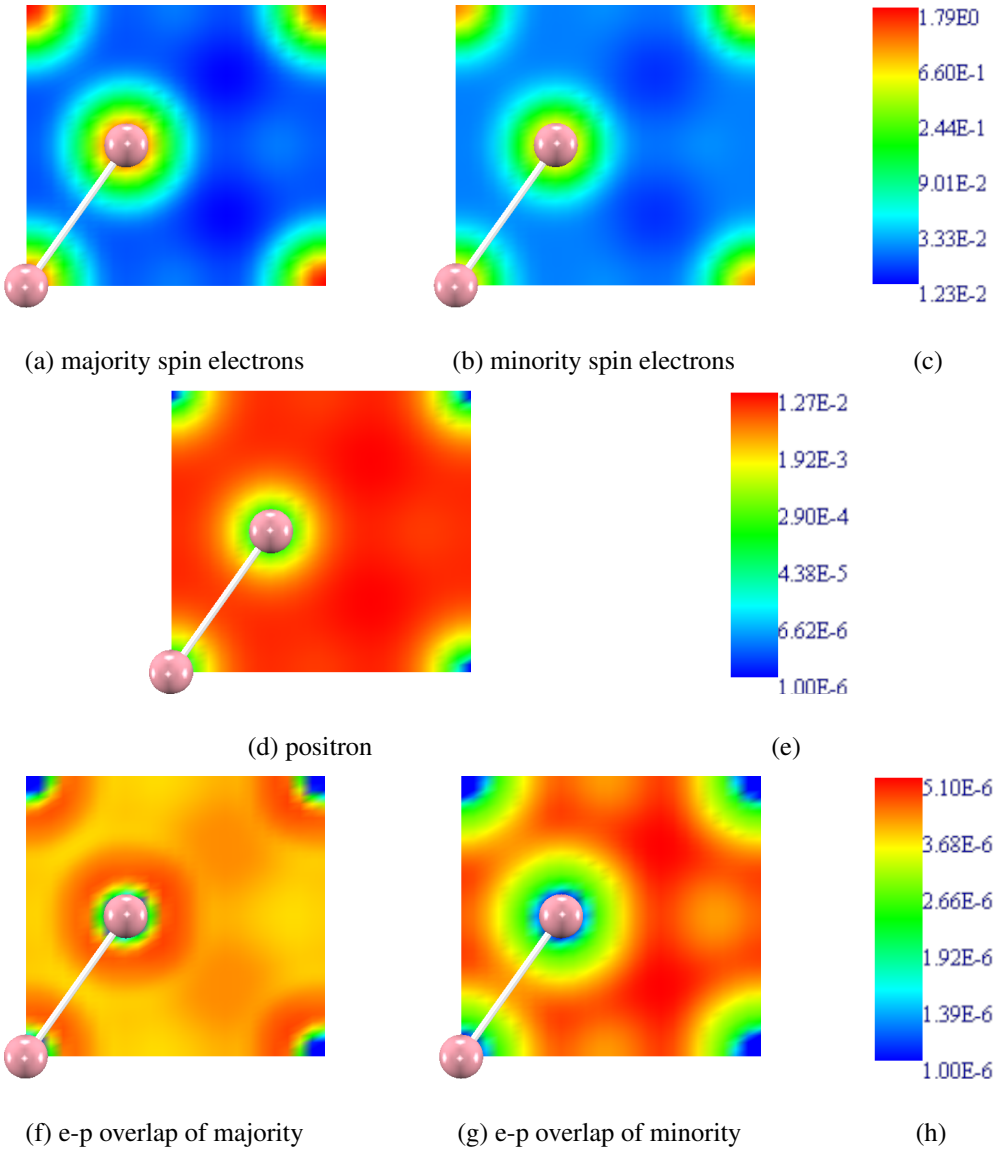

(a) majority spin electrons (b) minority spin electrons (c)

(d) positron (e)

(f) e-p overlap of majority (g) e-p overlap of minority (h)

Figure 4.5: Spin densities of electron ((a) and (b)), density of the positron (d), and electron-positron overlaps ((f) and (g)) in the case of Co of the [0100] direction. The units in (a), (b), and (d) are $e/(au)^3$, and those in (f) and (g) are $e^2/(au)^6$, respectively.

4.5 Conclusion

In this study, we carried out calculations on the lifetimes of spin-polarized positrons in Fe, Co, Ni and Gd by using EPDFT. First, we calculated the non-spin-polarized positron lifetimes and found that the calculated values are close to those of experiments. In the spin-polarized

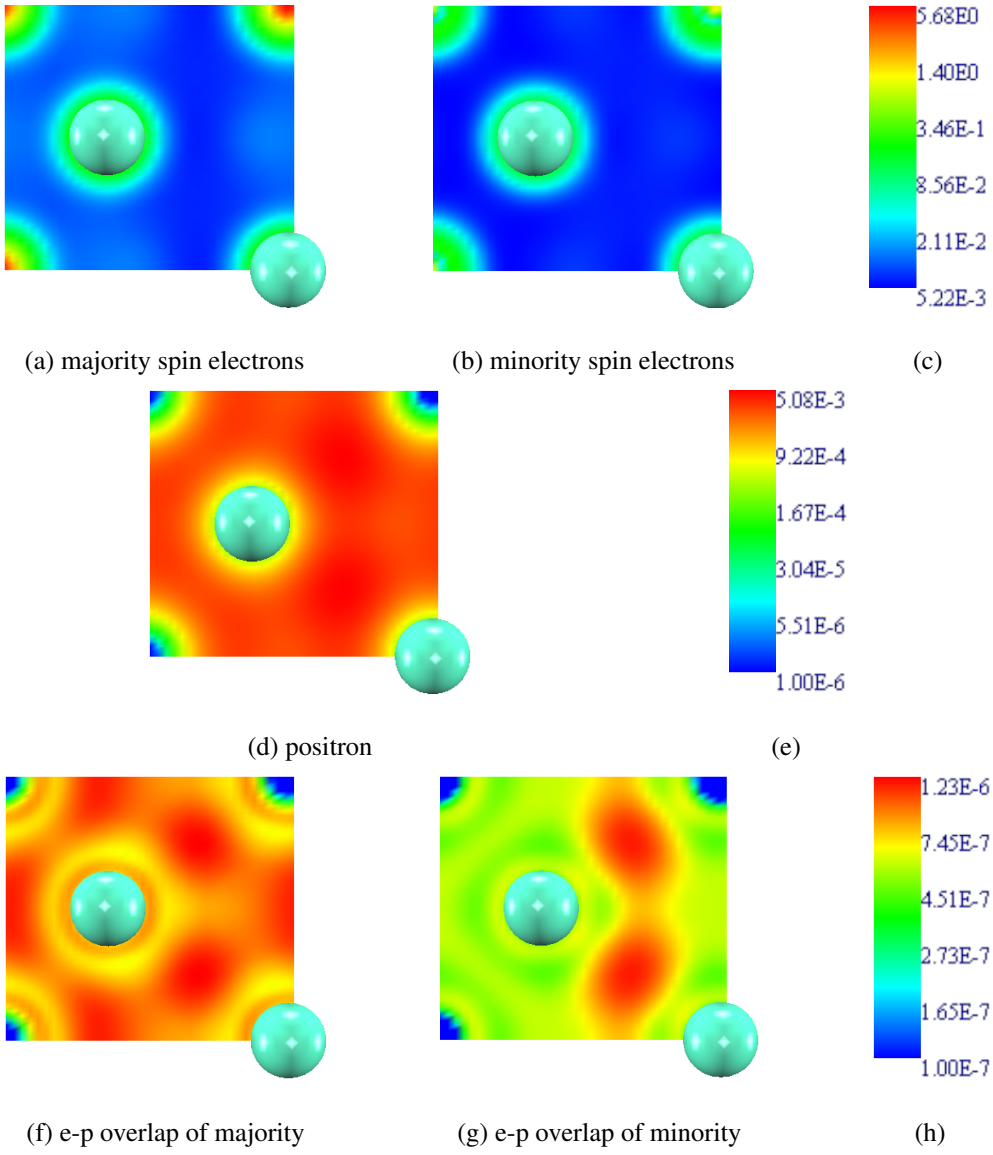

(a) majority spin electrons (b) minority spin electrons (c)

(d) positron (e)

(f) e-p overlap of majority (g) e-p overlap of minority (h)

Figure 4.6: Spin densities of electron ((a) and (b)), density of the positron (d), and electron-positron overlaps ((f) and (g)) in the case of Gd of the [0100] direction. The units in (a), (b), and (d) are $e/(au)^3$, and those in (f) and (g) are $e^2/(au)^6$, respectively.

positron lifetime calculations, we found that the lifetime differences ($\tau^{\downarrow} - \tau^{\uparrow}$) are 11.85 ps, 3.75 ps, -4.36 ps, and for Fe, Co, and Ni, respectively. The positive and negative values for Fe and Ni are consistent with results of 3γ experiment. It is suggested that the negative lifetime difference for Ni originates from unlocalized behaviour of minority electrons. We expect that when the magnetic moment of material is small, the negative lifetime difference tends to be

observed since the unlocalized behaviour of minority electrons are expected in other systems.

The agreement between theory and experiment suggests that the presently used calculational scheme is reliable for the lifetimes of spin-polarized positrons in electron spin-polarized materials. Therefore the present calculational scheme is expected to be an effective tool to analyze the experimental lifetimes. The observation of the momentum distribution of the spin-polarized positrons[34, 35] as well as the lifetime measurement emerges as a powerful tool to study spintronics. It is expected that the present calculational scheme is also useful to analyze the momentum distribution, though further theoretical study is invoked to confirm the reliability of the theory for the momentum distribution.

Chapter 5

Summary

5.1 Conclusions

In this paper, we study the two topics related to the semiconductor technology: First, we study the adatom-vacancy pair defects in graphene.

Then, we study the spin-polarized positron lifetimes in ferromagnetic metals Fe, Co, Ni and Gd. We here present conclusions for the two topics.

5.1.1 Adatom-Vacancy Pair Defects in Graphene

In the first study, we investigated the adatom-vacancy pair defects which is considered to be formed in single-walled carbon nanotubes (SWCNTs) by a low-energy electron irradiation measurement.[28]

The graphene which can be viewed as a SWCNT with a infinite radius, is considered as a suitable sample to know the phenomenon of the adatom-vacancy pair defects. We investigated the adatom-vacancy pairs in graphenes by carrying out first-principle calculations based on the spin-polarized GGA. The the healing barrier (0.06 eV) is found to be very small when the adatom is bonded to the nearest adatom of vacancy (geometry A).

We have also performed calculations for the cases that the adatom is located 4.26-5.54 Å far from the vacant site. The formation energies were found to be larger than that of geometry

A. Therefore, we expect that these defects are created when the energy injected into the pristine graphene is somewhat larger than that induces the adatom-vacancy pair of geometry A. We find that the healing barriers are 0.24-0.32 eV. These values are larger than that of the geometry A but are smaller than that of the adatom diffusion barrier (0.47-0.49 eV) [32, 33].

Among all the geometries, we find that the formation energy is getting larger when the distance of adatom from vacant site is larger. And geometries B and C have magnetic property.

Therefore,the followings are expected from the above results:

1. The adatom can be far from the vacant site, if the injection energy used in experiment increases. And some of these geometries are possible to have magnetic property.

2. As the healing barriers of the adatom-vacancy pair defects are expected to be smaller than that of the adatom diffusion barrier, this kind of defect can be healed under low temperature range where the adatom does not diffuse.

The experimental results from the hydrogen thermal desorption spectroscopy (at 44-70 K)[31], the low-energy electron irradiation (at 40-67 K)[28] suggest that the adatom-vacancy pair defects is healed at low temperature. Our results of healing barriers (0.06-0.32 eV) are consistent with these experimental results.

5.1.2 Positron Annihilation Study on Ferromagnetic Metals

In the second study, we carried out calculations on the spin-polarized positron lifetimes in ferromegnetic metals, Fe, Co, Ni and Gd by using EPDFT. First, we calculate the non-spin-polarized positron lifetimes and find that the calculated values are close to those of experiments. In the spin-polarized positron lifetime calculations, we found that the lifetime differences ($\tau^{\downarrow} - \tau^{\uparrow}$) are 11.85 ps, 3.75 ps, -4.36 ps, and 79.35 for Fe, Co, Ni, and Gd, respectively. The positive signs for Fe and Gd and the negative sign for Ni are consistent with results of 3γ experiment. From the analysing of the charge density of electron and positron, and the overlap of electron-positron, we suggest that the negative lifetime difference for Ni originates from delocalized behaviour of minority electrons. It is expected that when the magnetic moment of material is small, the negative lifetime difference tends to be observed since the delocalized behaviour of

minority electrons are expected in other systems.

From this study, the reliability of the calculation method based on the EPDFT is confirmed. Therefore, this calculational method is expected to be useful to analyse the experiment of SP-PAS.

Here, we conclude that the first-principles calculations are reliable and are expected to contribute to the development of new functional device.

5.2 Future Scope

5.2.1 Study of Atomic Defect in Functional Materials

Through the quantum mechanical simulations, we get useful results. We succeed in investigating the healing energies of the adatom-vacancy pairs in graphene.

Defects are important to study. The scheme we used is expected to be a suitable tool for studying the dynamics of atomic defects in nano materials. The dynamics of other kinds of

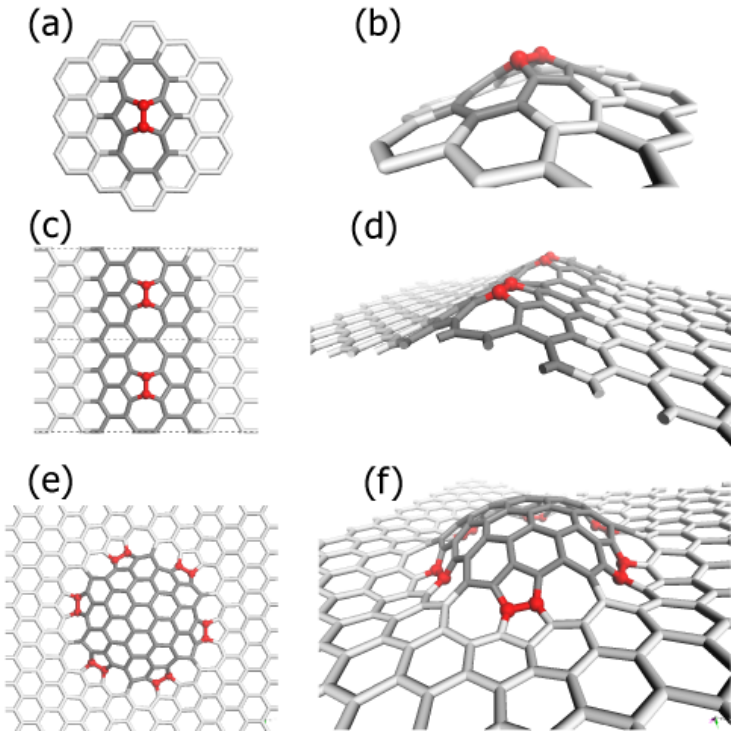

Figure 5.1: Defects in graphene.

defects is also expected to be studied efficiently by first-principles calculations, such as atomic defects in Si, CNTs, silicene, etc (Fig.5.1) [62].

5.2.2 Study of Spin-Polarized Positron Annihilation for Spintronics

We also succeed to calculate the positron lifetimes in the ferromagnetic metals, Fe, Co, Ni, an Gd by using EPDFT. The agreement between theory and experiment suggests that the presently used calculational scheme is reliable for the spin-polarized positron lifetimes in electron spin-polarized materials. Therefore the present calculational scheme is expected to be an effective tool to analyze the experimental lifetimes, such as bulk and thin film (half metals, ferromagnetic metals, and so on), vacancy-induced magnetism (DMS, SnO_2, CeO_2, ...), and surface and interface (magnetoregistance, spin hall, Rashba effect, topological insulator, spin-injection, etc.).

On the other hand, the momentum distribution of spin-polarized electrons are expected to be detected by spin-polarized positron annihilation experiment. The momentum distribution of spin-polarized electrons has more detail information than positron lifetime. Therefore, it is important to study this.

The observation of the momentum distribution of the spin-polarized positrons[34, 35] as well as the lifetime measurement emerges as a powerful tool to study spintronics. It is expected that the present calculational scheme is also useful to analyze the momentum distribution, though further theoretical study is invoked to confirm the reliability of the theory for the momentum distribution.

References

[1] R.M.Martin, Electronic Strucute: Basic Theory and Practical Methods (2004)

[2] http://www.ciss.iis.u-tokyo.ac.jp/.

[3] D. R. Hartree. The wave mechanics of an atom with non-Coulombic central I, II, III, volume 24:89,111,426. Proc. Cambridge Phil. Soc, 1928.

[4] P. Hohenberg, and W. Kohn: Phys. Rev. **B 136** (1964) B864.

[5] W. Kohn and L. J. Sham Phys. Rev. **A 140**, (1965) 1133

[6] A. D. Becke, Phys. Rev. **A 38**, (1988) 3098.

[7] J. P. Perdew, J. A. Chevary, S. H. Vosko, K. A. Jackson, M. R. Pederson, and C. Fiolhais, Phys. Rev. **B 46**, (1992) 6671.

[8] J. P. Perdew and Y. Wang: Phys. Rev. **B 46** (1992) 6671.

[9] J. P. Perdew, K. Burke, and M. Ernzerhof, Phys. Rev. Lett. **77**, (1996) 3865.

[10] Jorge Kohanoff. Electronic Structure Calculation for Solids and Molecules: Theory and Computational Methods (pp. 85-91). United Kingdom: Cambridge University Press (2006).

[11] P. S. Svendsen and U. von Barth. Gradient expansion of the exchange energy from second-order density response theory. Phys. Rev. B **54**, (1996) 17402.

[12] J. P. Perdew and K. Burke. Comparison shopping for a gradientcorrected density functional. Int. J. Quant. Chem. **57**, (1996) 309-319.

[13] D. R. Hamann, M. SchlNuter, and C. Chiang: Phys. Rev. Lett., **43**, (1979) 1494.

[14] D. Vanderbilt: Phys. Rev. B**41** (1990) 7892(R).

[15] A. J. Stone and D. J. Wales: Chem. Phys. Lett. **128** (1986) 501.

[16] A. V. Krasheninnikov, K. Nordlund, M. Sirvio, E. Salonen, and J. Keinonen: Phys. Rev. B **63** (2001) 245405.

[17] R. H. Telling, C. P. Ewels, A. A. El-Barbary, and M. I. Heggie: Nat. Mater. **2** (2003) 333.

[18] A. A. El-Barbary, R. H. Telling, C. P. Ewels, M. I. Heggi, and P. R. Briddon: Phys. Rev. B **68** (2003) 144107.

[19] A. V. Kransheninnikov, K. Nordlund, P. O. Lehtinen, A. S. Foster, A. Ayuela, and R. M. Nieminen: Phys. Rev. B **69** (2004) 73402.

[20] C. P. Ewels, R. H. Telling, A. A. El-Barbary, M. I. Heggie, and P. R. Briddon: Phys. Rev. Lett. **91** (2003) 025505.

[21] K. Yamashita, M. Saito, and T. Oda: Jpn. J. Appl. Phys. **45** (2006) 6534.

[22] M. Saito, K. Yamashita, and T. Oda: Jpn. J. Appl. Phys. **46** (2007) L1185.

[23] K. Nordlund, J. Keinonnen, and T. Mattila: Phys. Rev. Lett. **77** (1996) 699.

[24] P. O. Lehtinen, A. S. Foster, A. Ayuela, A. Krasheninnikov, K. Nordlund, and R. M. Nieminen: Phys. Rev. Lett. **91** (2003) 17202.

[25] M. Sternberg, L. A. Curtiss, D. M. Gruen, G. Kedziora, D. A. Horner, P. C. Redfern, and P. Zapol: Phys. Rev. Lett. **96** (2006) 075506.

[26] S. Okada: Chem. Phys. Lett. **447** (2007) 263.

[27] C. P. Ewels, R. H. Telling, A. A. El-Barbary, and M. I. Heggie: Phys. Rev. Lett. **91** (2003) 025505.

[28] K. Kanzaki, S. Suzuki, H. Inokawa, Y. Ono, A. Vijayaraghavan, and Y. Kobayashi: J. Appl. Phys. **101** (2007) 034317.

[29] K. Yamada, H. Sato, T. Komaguchi, Y. Mera, and K. Maeda: Appl. Phys. Lett. **94** (2009) 253103.

[30] O. Tonomura, Y. Mera, A. Hida, Y. Nakamura, T.Meguro, K. Maeda: Appl. Phys. A **74** (2002) 311.

[31] S.Arima, S.Lee, Y.Mera, S.Ogura, K.Fukutani, Y.Sato, K.Tohji and K.Maeda, Appl. Surf. Sci.**256**(2009) 1196-1199.

[32] P. O. Lehtinen, A. S. Foster, A. Ayuela, A. Krasheninnikov, K. Nordlund, and R.M. Nieminen, Phys. Rev. Lett. **91** (2003) 017202.

[33] Y. Uramoto and M. Saito: J. Phys. Soc. Jpn. **79**, (2010) 074605.

[34] A. Kawasuso, M. Maekawa, Y. Fukaya, A. Yabuuchi, and I. Mochizuki: Phys. Rev. B **83** (2011) 100406(R).

[35] A. Kawasuso, M. Maekawa, Y. Fukaya, A. Yabuuchi, and I. Mochizuki: Phys. Rev. B **85** (2012) 024417.

[36] M. Alatalo, M. Puska, and R. M. Nieminen: J. Phys.: Condens. Matter **5** (1993) L307.

[37] S. Berko and A. P. Mills: J. de. Phys. **32** C1 (1971) 287.

[38] T. W. Mihalisw and R. D. Parks: Phys. Lett. **21** (1966) 610.

[39] T. W. Mihalisw and R. D. Parks: Phys. Lett. **6** (1967) 210.

[40] T. Jarlborg, A. A. Manuel, Y. Mathys, M. Peter, A. K. Singh and E. Walker: J. Magn. Magn. Matt. **54-57** (1986) 1023.

[41] M. Matsumoto, K. Tomimoto and S. Wakoh: J. Phys. Soc. Jpn. **62** (1993) 2734.

[42] K. O. Jensen: J. Phys. Condens. Matter. **1** (1989) 10595.

[43] D. O. Welch and K. G. Lynn: Phys. Status. Solidi. B **77** (1976) 277.

[44] E. Boronski' and R. M. Nieminen: Phys. Rev. B **34** (1986) 3820.

[45] M. J. Puska, Ari P. Seitsonen, R. M. Nieminen: Phys. Rev. B **52** (1995) 15.

[46] L. J. Lantto: Phys. Rev. B **36** (1987) 5160.

[47] A. Nakamoto, M. Saito, T. Yamasaki, M. Okamoto, T. Hamada, and T. Ohno: Jpn. J. Appl. Phys. **47** (2008)2213.

[48] J. Arponen and E. Pajanne: Ann. Phys. (N.Y.) **121** (1979) 343.

[49] M. Saito, A. Oshiyama, S. Tanigawa: Phys. Rev. B **44** (1991) 19.

[50] H. Takenaka and D. J. Singh: Phys. Rev. B **77** (2008) 155132.

[51] Z. Tang , M. Hasegawa, T. Chiba, M. Saito, H. Sumiya, Y. Kawazoe and S. Yamaguchi: Phys. Rev. B **57** (1998) 12219.

[52] PHASE: http://www.ciss.iis.u-tokyo.ac.jp/dl/index.php

[53] I. Seki and K. Nagata: ISIJ Int. **45** (2005) 1789.

[54] H. Ibach and H. Lüth, Solid-State Physics (Springer-Verlag, Berlin, Heidelberg, 1995), 2nd ed.

[55] F. J. Darnell: Phys.Rev. **130** (1963) 1825.

[56] S. Berko: Positron Annihilation in Ferromagnetic Solids, in: Positron Annihilation, eds. A. T. Stewart and L. O. Roellig (Academic, New York, 1967) p.61.

[57] D. J. Chadi and K. J. Chang: Phys. Rev. B **38** (1998) 1523.

[58] T. Nagao, J. T. Sadowski, M. Saito, S. Yaginuma, Y. Fujikawa, T. Kogure, T. Ohno, Y. Hasegawa, S. Hasegawa, and T. Sakurai: Phys. Rev. Lett. **93** (2004) 105501.

[59] Y. Okamoto and Y. Miyamoto, J. Phys. Chem. B **105** , 3470 (2001).

[60] N. Jacobson, B. Tegner, E. Schroder, P. Hyldgaard, and B. I. Lundqvist, Comput. Mater. Sci. **24**, 273 (2002)

[61] A. Krasheninnikov, 2000, in: *Computational Methods for Material* Science, lecture notes, University of Helsinki

[62] Mark T. Lusk and L. D. Carr: Phys. Rev. Letters **100**, 175503 (2008)

Acknowledgments

Here, I would like to give thanks to many people. Without your help and support, this dissertation could not finished .

At first, I give my deepest gratitude to my supervisor, Prof. Mineo Saito. By his guidance, I could have worked out my dissertation. He has offered me valuable ideas, suggestions and criticisms with his profound knowledge in computational physics and rich research experience. His patience and kindness are greatly appreciated. Besides, he always puts high priority on our research and is willing to discuss with me anytime when he is available. I am very much obliged to his efforts of helping me complete the research.

I am also extremely grateful to Prof. Tatsuki Oda and Prof. Fumiyuki Ishii who have offered me many valuable ideas and comments about our research. I also give thanks to Prof. Hidemi Nagao and Prof. Shinichi Miura who let me know more about our research and know more about my possibility and ability. More than that, I give thanks to Dr. Astuo Kawasuso for helpful discussions in the positron lifetime study.

Thanks are also due to my laboratory members, who never failed to give me great encouragement and suggestions. Especially thanks to my friends, Ms. Patricia Hotma Minar Lubis, Mr. Kazunori Nishida, Mr. Mohammad Shafiul Alam and Mr. Weihua Shi for their help not only related to my research. I also would like to express my sincerely thanks to my parents for their understanding, encouragement and support.

At last but not least, thanks a lot to the programmers of the code PHASE and to the people working for the supercomputer platforms (T2K open supercomputer, ISSP and FX10 in University of Tokyo, MIC in Kanazawa University) where we perform simulations.